NACA RM A55I21

`3 1176 00099 0177`

NACA

RESEARCH MEMORANDUM

A DESCRIPTION OF THE AMES 2- BY 2-FOOT TRANSONIC

WIND TUNNEL AND PRELIMINARY EVALUATION

OF WALL INTERFERENCE

By Joseph M. Spiegel and Leslie F. Lawrence

Ames Aeronautical Laboratory
Moffett Field, Calif.

CLASSIFICATION CHANGED

UNCLASSIFIED

To_____

By authority of _τ RN-118_____ Date _July 26, 1957_

𝑛ACA Rec abs

Amt 8-21-57

NATIONAL ADVISORY COMMITTEE
FOR AERONAUTICS
WASHINGTON
January 20, 1956

NATIONAL ADVISORY COMMITTEE FOR AERONAUTICS

RESEARCH MEMORANDUM

A DESCRIPTION OF THE AMES 2- BY 2-FOOT TRANSONIC

WIND TUNNEL AND PRELIMINARY EVALUATION

OF WALL INTERFERENCE

By Joseph M. Spiegel and Leslie F. Lawrence

SUMMARY

The Ames 2- by 2-foot transonic wind tunnel, an aeronautical research facility in which the Mach number can be varied continuously from low subsonic values up to 1.4, is described. An adjustable nozzle for producing supersonic velocities and a form of perforated-wall test section for alleviating wall interference effects are utilized. Although no attempt was made to thin the wall boundary layer ahead of the test model, control of test section plenum-chamber pressure by means of a suction pump is shown to be an effective means of reducing the main compressor pressure ratio requirements and over-all power consumption.

Surveys of the empty test section indicate that the local Mach number variations are within ±0.003 over a 20-inch length of test section, up to 1.35 Mach number, and no over-all longitudinal gradients are present in this region.

Wall interference is evaluated by comparing force and pitching-moment measurements on three different sizes of a wing-body configuration, having frontal projected areas of 0.09, 0.51, and 1.15 percent of the test section area. The tests indicate that large reductions in interference are possible in the subsonic and low supersonic speed ranges by use of the perforated walls, as compared to nearly solid walls which are sufficiently perforated in the corners to prevent choking. From these tests it is concluded that the wall interference is small for a model having a projected frontal area of 1/2 percent of the cross-sectional area of the test section and a wing-span-to-tunnel-height ratio of one-half.

INTRODUCTION

In the development of transonic wind tunnels utilizing partly open test-section walls, the primary objectives are to obtain uniform flow in the test region and to minimize wall interference on the test models. The various configurations that have evolved in recent years to achieve these objectives are distinguished by: (1) the type of partly open walls forming the test section, (2) the manner in which supersonic flow is produced, and (3) the extent to which the thickness of the boundary layer on the test-section walls is controlled.

Two types of partly open walls have generally been used - longitudinal slots, and uniformly distributed perforations. Two methods also have commonly been employed for the generation of supersonic flow - expansion of an initially sonic flow through the partly open walls of the test section into a surrounding chamber (see, e.g., refs. 1 and 2), and expansion through a convergent-divergent nozzle immediately ahead of the test section (ref. 3). Concerning the control of the boundary-layer thickness, it is known that thinning the boundary layer is desirable because of increased attenuation of reflected disturbances (refs. 4 and 5). As a practical matter, however, the additional equipment required for this purpose may sometimes preclude test-section boundary-layer control.

The Ames 2- by 2-foot transonic wind tunnel was designed about the option consisting of (1) a form of perforated-wall test section, (2) a convergent-divergent nozzle for supersonic flow generation, and (3) no provision for thinning of the test-section boundary layer upstream of the test models. However, a suction pump of limited capacity is used to aid in controlling the pressure in a plenum chamber surrounding the perforated test section. These choices evolved largely from consideration of the analysis and data presented in reference 3 and unpublished test data previously obtained with a 5- by 5-inch model test section.

In this paper the principal features of the Ames 2- by 2-foot transonic wind tunnel are described. In addition, since many of the adjustments required to establish uniform flow at transonic Mach numbers are peculiar to this type of tunnel, the basic principles underlying them are briefly discussed. The investigations conducted to establish the adequacy of this test-section configuration as a useful facility for aerodynamic research are also recounted. The accomplishment of this latter objective required extensive measurements of the flow field and an evaluation of the wind-tunnel wall interference. Since theoretical methods are inadequate at present for predicting wall-interference effects, conclusions are based upon comparisons of the experimentally measured aerodynamic characteristics of three scaled models of the same wing-body configuration.

<p style="text-align: center">NOTATION</p>

C_D drag coefficient, $\dfrac{\text{total drag less base drag}}{qS}$

C_L lift coefficient, $\dfrac{\text{lift}}{qS}$

C_m pitching-moment coefficient referred to quarter point of mean aero-
dynamic chord, $\dfrac{\text{pitching moment}}{qS\bar{c}}$

M   Mach number

P_O power required by main-drive compressor

P_S power required by main-drive compressors with auxiliary suction

P_P power required by suction pump

P_T total power, $P_S + P_P$

p   static pressure

R   Reynolds number

S   total wing area, including that blanketed by fuselage

b   wing span

c   wing chord

$\bar{c}$ wing mean aerodynamic chord, $\dfrac{\displaystyle\int_0^{b/2} c^2 dy}{\displaystyle\int_0^{b/2} c\, dy}$

w_P mass flow through suction pump

w_O mass flow through main-drive compressor

q   free-stream dynamic pressure

r   radius of body

r_O maximum body radius

α   angle of attack

η   compressor efficiency

PART I - DESCRIPTION OF THE WIND TUNNEL

THE WIND-TUNNEL CIRCUIT

The Ames 2- by 2-foot transonic wind tunnel is of the closed-return, variable-density type with a test section having perforated walls. A schematic drawing of the tunnel circuit and of the auxiliary equipment is presented in figure 1. As indicated in this figure, power is supplied to the air stream by a two-stage axial-flow compressor, each stage of which is composed of two counterrotating sets of blades. These fans are driven by four 1000-horsepower, water-cooled, squirrel-cage induction motors. Motor speed is controlled by varying the frequency of the input current. Figure 2 is a sectional perspective view of the nozzle, test section, and diffuser region of the wind tunnel.

Nozzle

A variable geometry convergent-divergent nozzle is used to generate supersonic Mach numbers up to 1.4. The nozzle is bounded by two plane parallel walls and two flexible-plate walls of varying thickness in the axial direction. As described in reference 3, the plate thickness is varied along the length such that when the plate is deflected by a single jack the deflection curve approximates the nozzle shape corresponding to a given Mach number. In the present instance the plate thickness distribution was selected to yield the deflection curve corresponding to the nozzle shape calculated by the method of characteristics to produce a uniform flow field of 1.25 Mach number at the entry to the test section. For nozzle shapes other than this the flow field is only approximately uniform at the entrance to the test section.

Test Section

The test section is 2 feet square in cross section and 4 feet long. The vertical side walls are parallel, but the top and bottom walls are diverged slightly to compensate approximately for the growth of the boundary layer. The test section is enclosed by a pressure-tight cylinder which forms a plenum chamber to maintain uniform pressure on the four side walls (see fig. 2).

The walls of the test section are perforated with triangular holes as shown in figures 2, 3, and 4(a). The function of the perforations is to permit a fraction of the air in the test section to bypass the test model by flowing through the porous walls into the plenum chamber. This condition more nearly simulates free flight than do solid walls, because some of the streamlines, in effect, pass through the walls (see ref. 3). Subsonic blockage effects are thereby relieved and reflected shock waves are attenuated at supersonic speeds. The triangular shape was selected to achieve sweepback of the edges of the holes and to thereby minimize stream disturbances from this source at supersonic speeds. The side walls are constructed of alternately assembled aluminum alloy strips and plate glass rails 1-1/4 inches deep. Glass is employed to permit visual observation of the flow. The top and bottom walls are the same except that the rails are constructed of pressed-wood die stock 1-3/4 inches deep. The triangular holes are formed from V-shaped corrugations cut in each side of the aluminum strips and closed on the third side by the surface of the adjacent rail. The porosity resulting from this configuration is 6 percent (i.e., open-to-total-area ratio times 100). There are 16 aluminum strips per side wall. This number is shown in reference 3 to be sufficient when the wall boundary layer is not removed.

Effuser

The stepped opening at the entry to the diffuser (figs. 2 and 4(b)) is called the "effuser" and serves to vent the plenum chamber to the main stream. The ejector action of the main stream flow on the effuser produces an outflow of air from the plenum chamber that is necessary to control the pressure level in this chamber. Pressure control is necessary at supersonic speeds in order to prevent the low-energy air, entering the plenum chamber from the test section due to the blockage of the model, from re-entering the test section upstream of the model. At Mach numbers near unity the step and gap of the effuser prevent "choking" of the flow at the end of the test section by providing area compensation for air entering the diffuser from the chamber, and for the model support. The effuser settings found to be the most satisfactory (for the size of model shown in fig. 3) for controlling the pressure in the chamber are presented in figure 4(b).

The effuser is of very low efficiency; hence it is supplemented by an auxiliary suction pump (fig. 1), consisting of a centrifugal compressor of sufficient capacity to remove up to 1-1/2 percent of the main tunnel mass flow at Mach number of unity. This size of compressor was used only because it was available at the laboratory when this wind tunnel was built.

Model Support

Models are sting-supported from a horizontal strut in the diffuser, as indicated in figures 2 and 3. The maximum angle of attack attainable with straight stings is $\pm 8^\circ$; for higher angles of attack bent stings are utilized. The angle-of-attack mechanism is constructed in such a manner as to maintain the model center of rotation within 1/32-inch of the tunnel center line for straight stings. With the model rotated 90° on the sting, angles of yaw of $\pm 8^\circ$ may be encompassed.

AUXILIARY EQUIPMENT

Auxiliary equipment is provided for controlling the pressure, temperature, and humidity in the wind tunnel. The tunnel is evacuated by use of two rotary-type, single-stage vacuum pumps mounted in parallel. Air is supplied to the tunnel from a storage tank, charged with dry air by a make-up compressor and air drier. The air drier is an adsorptive type using silica gel as the active agent, and is capable of maintaining the absolute humidity of the air at a value less than 0.0003 pound of water per pound of air. The ratio of storage tank to tunnel volume is 1/5; maximum tank pressure is 75 pounds per square inch gage. The temperature in the wind tunnel is controlled by means of cooling coils located, as shown in figure 1, downstream of the drive motors.

INSTRUMENTATION

Model Balance

A representative six-component resistance-type strain-gage balance used to measure model lift, drag, side force, and pitching, yawing, and rolling moments is illustrated in figure 5. The balance, which is of the flexure pivot type, is designed to be housed entirely within the model body.

Mach Number Indication

Mach number is determined from the static pressure in the test-section plenum chamber and the static pressure in the upstream settling chamber. The plenum-chamber pressure was calibrated against the test-section static pressure determined from axial tube surveys and found to be essentially the same.

Mach number is indicated automatically to an accuracy of ±0.001 by means of a "Mach meter." This device consists basically of two barometric-type mercury U-tubes, one of which measures settling-chamber static pressure, and the other plenum-chamber static pressure. Encircling one side of each U-tube, and mounted on a servo-driven lead screw, is a differential transformer which automatically follows an iron float on the mercury column. The positions of these lead screws indicate the pressures; the ratio of these pressures is automatically computed and indicated.

Schlieren Apparatus

The surfaces of the plate glass rails in the sides of the test section are not sufficiently plane or parallel to permit the use of conventional black and white schlieren. Each rail refracts the light beam in a different direction so that there is no common focal point for the image of the light source. As a result, for any given position of the knife edge, the schlieren pattern of the flow field is nonuniformly illuminated. Changing the position of the knife edge brings the field into focus for other rails and loses it for the original ones. These conditions seriously reduce the usefulness of the conventional black and white schlieren for research work.

For these reasons a colored schlieren system is employed similar to that described in references 6 and 7. With this arrangement the slit replacing the knife edge at the image focal point can be adjusted so that a schlieren field is obtained for all rails simultaneously. The variable amounts by which the light rays are diverted by the various rails leads, however, to a multicolored background. A complete picture of the shock-wave pattern is nevertheless obtained under all flow conditions for a single position of image slit.

OPERATION

Mach Number Control

The Mach number in the test section at subsonic speeds is controlled by varying the compressor pressure ratio in the same manner as is done for a conventional solid-wall subsonic wind tunnel. At supersonic speeds Mach number variation is achieved by control of the flexible nozzle shape, the compressor pressure ratio, and, to some extent, the pressure in the plenum chamber surrounding the test section. The Mach number at the nozzle exit is determined, of course, by the nozzle shape, but the pressure in the plenum chamber finally determines the average Mach number in the test section. In general, when the plenum-chamber pressure is lower than that of the nozzle exit, air will flow out of the test section into the plenum

chamber, resulting in a higher average test-section Mach number than that at the nozzle exit. When the plenum-chamber pressure is higher than that at the nozzle exit, the reverse is true. The basic criterion for tunnel operation at supersonic Mach numbers that has been selected is to maintain the plenum-chamber pressure equal to that at the nozzle exit for a given nozzle setting. This procedure minimizes flow in or out of the test section ahead of the model and thereby minimizes disturbances that emanate from the beginning of the perforated region. The maximum attainable test-section Mach number is 1.4.

The effuser alone actually affords sufficient control of the plenum-chamber pressure to control the test-section Mach number, but it is by nature a device of very low efficiency. It is therefore supplemented with an auxiliary suction pump which removes air from the plenum chamber (in place of allowing it to be aspirated out through the effuser) and returns it to the air stream in the diffuser region of the circuit. The use of this auxiliary suction pump results in considerably lower pressure-ratio requirements from the main compressor for supersonic operation. It is to be noted that, by virtue of the limited capacity of the suction pump (approximately 1-1/2 percent of the tunnel mass flow at a Mach number of unity) no attempt is made to employ the pump to thin the test-section-wall boundary layer.

Reynolds Number

As in any other wind tunnel, the attainable Reynolds number is governed by model size and the power available in the drive motors. The maximum Reynolds number per foot presently attainable in the 2- by 2-foot transonic wind tunnel is shown in figure 6 as a function of Mach number for a representative wing-body combination at angles of attack of $0°$ and $8°$. The inflections of the curves in the region of 1.05 Mach number coincide with the application of auxiliary suction to the test-section plenum chamber. The noticeable increase in attainable Reynolds number is the result of main-drive power savings afforded by auxiliary suction.

PART II - CALIBRATION OF THE WIND TUNNEL

OBJECTIVES

To appraise the usefulness of this wind tunnel for three-dimensional model testing, surveys were made of the tunnel-empty Mach number distribution, and the interference of the test-section walls on the model test data was assessed. The wall-interference tests were initiated with two objectives in view: (1) to determine the alleviation of interference, and

(2) to determine the maximum permissible model size for three-dimensional model testing. These objectives were accomplished by comparing the lift, drag, and pitching moments of three different scaled models of a wing-body configuration measured in the porous test section with corresponding values obtained with quasi-solid side walls sufficiently open at the corners to prevent choking.

APPARATUS

The Mach number distribution in the test section was measured by means of an axial tube extending from the settling chamber downstream through the nozzle, test section, effuser, and terminating in the diffuser. This tube, 1/2-inch in diameter, has 14 longitudinal pressure-measuring stations on 12-inch centers. At each measuring station there are three static orifices located at 120° intervals on the periphery. The supporting structure at each end was designed so that the axis of the tube could be located at any cross-sectional coordinate of the test section in the absence of the model support; and, through external controls, the tube could be translated to obtain axial surveys at all longitudinal stations.

All pressures were measured with tetrabromoethane manometers to the nearest 0.03 inch.

Three sizes of the wing-body configuration shown in figure 7 were employed. They blocked 0.09, 0.51, and 1.15 percent of the tunnel cross section (based on projected frontal area of models). The corresponding wing-span-to-tunnel-width ratios were 19.6, 45.6, and 68.4 percent. Hereinafter, these models are referred to as the small, medium, and large models. A photograph of the medium model mounted in test section is shown in figure 3.

The large differences in the size and force reactions of the three models required the use of a different balance with each model. The balance used with the small model was a bearing-pivot-type strain-gage balance located in the sting, outside of the model. It was used to measure lift and drag forces only - pitching moment was obtained from a separate strain-gage beam mounted inside the fuselage. Forces on the medium and large models were measured with the flexure-pivot balances of the type previously described. The sting supports of all three models were geometrically similar in order to preclude discrepancies in the measured data from differences in support interference. In the case of the small model a shroud was used to cover the actual sting and external balance so as to obviate aerodynamic tares.

TESTS

Mach Number Surveys

Measurements of tunnel-empty Mach number distributions were made at
Mach number increments of 0.05 in the range from 0.80 to 1.40. Settling-
chamber pressure was maintained at 15.0 pounds per square inch absolute,
and temperatures held between 90° and 120° F. Local Mach numbers were
measured at 2-inch intervals throughout the length of the test section
at 13 cross-sectional stations. The cross-sectional region surveyed was
6 inches either side of the vertical center line, and between 4 inches
and 8 inches above the horizontal center line. Observations closer than
4 inches to the horizontal center line were prohibited by mechanical inter-
ference between the axial tube and the horizontal strut containing the
angle-of-attack mechanism (see fig. 2).

Since the orifices on the tube were spaced at 12-inch intervals, six
positions, 2 inches apart, sufficed for each survey. Data were also taken
at the seventh 2-inch increment, however, to determine whether any dis-
crepancy existed in the pressures measured by adjacent orifices at iden-
tical positions in the air stream. Six of the 14 orifice stations avail-
able were required to span the length of the test section and portions of
the nozzle and diffuser of interest.

The local Mach number corresponding to each free-stream static-
pressure reading was calculated using settling-chamber static pressure
for total head. A reference Mach number, corresponding to the plenum-
chamber pressure, was computed for each of the 2-inch incremental loca-
tions of the axial tube. The local Mach numbers were then corrected to
account for the change in reference Mach number taking place during each
survey by adding or subtracting the difference between the two reference
Mach numbers corresponding to the local Mach number. The magnitude of
this correction never exceeded 0.001 Mach number.

A second correction was necessitated by the difference in pressures
measured with adjacent orifices at the same axial position. This cor-
rection was considered equal to the difference in Mach numbers computed
from pressure readings obtained with adjacent orifices at the same stream-
wise location. It was applied to all six readings of five of the six
orifices; readings from the sixth orifice (the readings from which most
closely agreed with plenum-chamber static pressure) were left unchanged.
These Mach number corrections were of the order of 0.003 and did not
exceed 0.007.

Wall-Interference Tests

Lift, drag, and pitching moments were obtained for each of the models in the Mach number range 0.60 to 1.30 at Reynolds numbers of 0.6 and 1.5 million based upon the mean aerodynamic chord, and at angles of attack varying from -5° to +13° approximately. The measured drag was adjusted to correspond to a condition of free-stream pressure acting at the model base.

The estimated accuracies of the measurements, based upon the ability to repeat data, are within the limits given in the following table:

	α deg	c_L	c_D	c_m
Small model	±0.10	±0.020	±0.0021	±0.001
Medium model	±.02	±.012	±.0006	±.005
Large model	±.02	±.004	±.0006	±.001

Replacement of the porous side walls with quasi-solid ones was effected by sealing all longitudinal rows of perforations, except two rows in each corner, with cellophane tape. By this means the open area was reduced from 6 percent to 3/4 percent, which was sufficient to prevent choked flow for all three sizes of models throughout the angle-of-attack and Mach number ranges investigated.

RESULTS AND DISCUSSION

Tunnel-Empty Flow Characteristics

In figures 8(a) and (b) are shown tunnel-empty longitudinal Mach number distributions which were measured 4 inches above the tunnel center line. Transverse Mach number variations were found to be negligible in the test region and therefore data at other cross-sectional stations have not been presented. To disclose the sources of the larger longitudinal variations, these figures include data for the latter portion of the nozzle and the initial portion of the diffuser as well. From figure 8(a) it is clear that, at subsonic speeds, from stations 5 to 40, local Mach number variations are practically nonexistent. In the supersonic range, for Mach numbers up to 1.35, between stations 20 and 49 (fig. 8(b)) the variations, while larger, are still inconsequential, amounting to less than ±0.003. At 1.4 Mach number, the region between stations 22 and 49 shows variations within ±0.005. There are, furthermore, no over-all gradients evident at any Mach number. It is thus evident that at all Mach numbers up to 1.35, the region from stations 20 to 40 - a distance of 20 inches - is suitable

for model testing. Between 1.35 and 1.40 Mach number the region suitable
for testing is 2 inches shorter on the upstream end, and the Mach number
variation is somewhat greater.

It is to be observed that the variations in Mach number occurring
outside this test region (stations 20 to 40) are entirely different in
the subsonic and supersonic Mach number ranges. At subsonic Mach numbers,
the principal variation consists of a gradient at the downstream end of
the test section, beginning at station 38 and increasing in magnitude and
extent with Mach number.[1] Increasing the rate of air removal from the
plenum chamber by use of the suction pump has been found to aggravate the
gradient. At supersonic speeds this gradient is entirely absent from the
test section, even with the use of auxiliary suction; but there are pro-
nounced Mach number variations at the upstream end of test section, the
magnitudes of which increase with Mach number. In addition, at $M = 1.25$
and above, an overexpansion of significant and increasing magnitude appears
in the nozzle itself.

There is a plausible explanation for the disappearance of the gradi-
ent at the downstream end of the test section at supersonic Mach numbers,
based upon the fact that at subsonic speeds, expanding streamlines are
accompanied by a decelerating flow, and at supersonic speeds, by accel-
erating flow. At subsonic speeds the passage of air out of the main stream
into the plenum chamber via the perforations in the walls causes the stream
to slow down. This slowing down increases the free-stream static pressure
which, in turn, increases the amount of air flowing from the main stream
into the plenum chamber. An initially unstable situation therefore exists,
for which equilibrium is eventually attained, but only after a large Mach
number gradient appears at the downstream end of the test section. The
fact that the gradient appears only near the end of the test section is
predicted by mathematical analysis and substantiated by experimental data
in reference 8. At supersonic Mach numbers, conditions are reversed and
the gradient in the test section is not evident. Passage of air from the
main stream to the plenum chamber causes the Mach number to increase, the
free-stream static pressure to decrease, the rate of flow of air into the
plenum chamber to diminish, and the Mach number gradient of the main stream
to correct itself.

The Mach number variations occurring in the upstream portion of the
test section at supersonic Mach numbers can be traced to their source by
use of Mach lines. By so doing it is found that the variations originate
principally in disturbances at the boundary of the flow in the vicinity

---

[1]It has been found that this gradient region can be moved farther
downstream in either of two ways; first, by modifying the effuser so as
to reduce the step and gap (fig. 4(b)), and second, by extending the test
section at the downstream end. The effect of reducing the step and gap
is indicated by the diamond symbols in figure 8(a). The diffuser wall
divergence just downstream of the effuser is 1° for both settings.

of station 1. This result is indicated by the dashed line appearing in figure 8(b), marking the farthest downstream point at which disturbances from this source intersect the axial survey line. Measurement of the physical discontinuity between the nozzle and side walls of the test section disclosed it to be too small (less than 0.005 inch) to furnish an explanation. The variations are therefore attributed to the inability to attain perfect pressure equalization at the beginning of the perforated region, and it is considered possible that by reducing the porosity in the upstream portion of the test section the magnitude of the variations would be significantly decreased.

The Mach number variations occurring in the nozzle result from the fact that the plates forming the nozzle were designed for 1.25 Mach number (see "Nozzle" section), and it is to be expected that the flow would become progressively worse above this Mach number. It is to be noted that at M = 1.35 and below, all disturbances originating at station 1, as well as those arising in the nozzle, are practically eliminated after the first impingement on the porous side walls of the test section.

Wall Interference

The general term "wall interference" is used in this report to mean any effect on the aerodynamic forces of the model resulting from the presence of the tunnel walls. Wall interference does not include support interference, which for this tunnel is reported in reference 9. The support interference that does exist in the measured data is invariant between the three models because of geometric similitude (see "APPARATUS" section). In the following comparisons force data for the small model are assumed to be nearly interference-free because the blockage was only 0.09 percent of the cross-sectional area of the test section. Also, by tracing Mach lines, it is estimated that this model is completely free of reflected disturbances above 1.1 Mach number.

The basic data, from which both the alleviation of wall interference and the maximum model size permissible for routine testing are estimated, are presented in figures 9 through 17. In these figures lift coefficient is plotted as a function of angle of attack, of drag coefficient, and of pitching-moment coefficient for each of the three sizes of wing-body models tested. For purposes of analysis these data have been cross-plotted in figures 18 through 22 so that lift coefficient, drag coefficient, and pitching-moment coefficient are shown and compared as functions of Mach number for constant values of angle of attack.

It is to be noted in passing that, in general, the lift-coefficient versus angle-of-attack curves (figs. 9, 12, and 15) pass through the origin and the drag polars are symmetrical, thus indicating an absence of stream angularity in the case of these symmetric models (models were also tested

in the inverted position to check for symmetry). Furthermore, since
longitudinal variations in Mach number are a measure of stream angularity
changes and since this variation is shown by the data of figure 8(b) to
be small, the stream angularity at other locations of the test section
must also be small.

Because it was not possible to test the small model at 1.5 million
Reynolds number, corrections were applied to the results for the small
model on the cross plots before comparing them with those for the other
two sizes. These corrections were estimated by assuming that they would
be equal to the difference between the results measured for the medium
model at $R = 0.6$ million and at $R = 1.5$ million. This correction, of
course, is based on the assumption that the magnitude of the wall inter-
ference is not significantly affected by the change in wall boundary-
layer thickness corresponding to this change in Reynolds number. Since
the thickness of this boundary layer, which affects reflected disturbances,
varies only as the 1/5th power of the Reynolds number, the assumption is
considered reasonable.

In figure 18 are shown the cross-plotted data for the medium model
corresponding to 0.6 and to 1.5 million Reynolds number. It is apparent
that the results generally agree well except in three particular ranges:
(a) the Mach number range of 0.9 to 0.98 for C_L and C_m, (b) the subsonic
Mach number range for minimum C_D, and (c) the high angle-of-attack range
for all components. All of these ranges are known to be sensitive to the
state of the boundary layer, and therefore to changes in Reynolds number.
The differences of figure 18 have been applied directly to the results
for the small model to obtain the data plotted in figures 19 through 21.

Alleviation of wall interference.- In figure 19 comparative data are
presented to show the alleviation of wall interference for the large model
obtained by the use of the 6-percent-open-area walls, as contrasted with
results for the practically solid walls which had 3/4-percent-open area
at the corners to prevent choking. These data demonstrate that large
reductions in wall interference are obtained for all components throughout
the Mach number range from 0.6 to 1.3. The gains are shown most emphati-
cally by the C_D plots, which indicate reductions in reflected-wave
interference of as much as 80 percent at Mach numbers between 1.0 and 1.3.
Drag, of course, is very sensitive to boundary-reflected disturbances due
to the additive effect of the waves reflecting from opposing walls, par-
ticularly at angles of attack close to zero.

The pitching-moment-data results are somewhat anomalous. For example,
in figure 19(c), the quasi-solid-wall data are in closer agreement with
the small model data for 6° and 8° angles of attack at high subsonic speeds
than are the data for the 6-percent-open walls. Other discrepancies can
be noted at high angles of attack in the subsonic speed range. No reason-
able explanation of these differences has been found; it can only be

suggested that the point of boundary-layer transition on the test bodies may vary between the different models due to a difference in roughness, even though the Reynolds numbers are the same.

Despite the reduction in interference attained by the use of the 6-percent-open walls, inspection of figure 19 reveals that a considerable amount of residual interference still remains for this model, assuming the small model data to be interference free. This observation is particularly true in the supersonic Mach number range, where discrepancies of as much as 15 percent in C_L, 16 percent in C_D, and 19 percent in C_m are evident. In all three parts of the figure, at practically all angles of attack, a rather prominent, localized increase in force and moment coefficients, for the large model lying in the range of 1.05 to 1.20 Mach number, will be noticed. This increase is most pronounced in the lift curves (fig. 19(a)), but it is quite evident in the drag and pitching-moment curves as well. With increasing angle of attack, it tends to shift in the direction of higher Mach number. These localized increases are attributed to disturbances in the flow caused by reflections from the test-section walls, of the shock and expansion waves emanating from the wing. For the Mach number range under discussion this shock wave is detached; hence, the stronger it becomes (as the angle of attack becomes greater) the farther forward of the model it lies and the higher the Mach number required for its reflections to intersect a given point on the model.

Information similar to that appearing in figure 19 for the large model is shown in figure 20 for the medium model. Again it is observed that the 6-percent-open walls produce much less interference. As for figure 19 the plots of C_D show the greatest reduction in wall interference, and it is noteworthy that the maximum reduction again approximates 80 percent. Throughout the entire Mach number range, however, the residual interference is very much less than that for the large model.

The maximum percentage differences between the small and medium model data (6-percent-open walls) at supersonic speeds can be quoted as follows: for C_L it is as much as 5 percent (0.016 at $M = 1.21$, $\alpha = 4^\circ$); for C_D it is as much as 11 percent (0.0025 at $M = 1.03$, $\alpha = 0^\circ$); and for C_m it is as much as 13 percent (0.008 near $M = 1.11$, $\alpha = 6^\circ$). The reliability of these differences, as an indication of wall interference, however, must be accepted with some reservation because the maximum, combined, experimental errors are of the same order of magnitude as the differences themselves (see "TESTS"). Therefore, to the accuracy of these measurements, the data for the medium model do not require any wall-interference corrections. At subsonic speeds differences of about 0.01 in C_m occur at 8° angle of attack. Correspondingly, this discrepancy is evident to a lesser extent in both lift and drag. This result is not believed to be any effect of wall interference, but rather a particular sensitivity to boundary-layer transition as previously mentioned.

A more accurate evaluation of the effects of wall interference on the results for the medium size model will be possible when the model and balance can be tested in a larger facility at a common Reynolds number. The problem of wind-tunnel wall corrections may then be re-examined.

Choice of model size.- To determine the largest size of model for which reliable data can be obtained in this 2-foot-square, 6-percent-open, porous-wall test section, the appropriate lift, drag, and pitching-moment curves for each of the three model sizes appearing in figures 19 and 20 are compared again in figure 21. It is apparent that the medium size model is about as large as should be tested, and the results for this model, when compared with those for the small model, are very satisfactory. Note that for the large model, in the supersonic range between Mach numbers 1.05 and 1.20, the lift and drag data particularly, and the pitching-moment data to a lesser extent, all show serious discrepancies.

The conclusion that valid data are provided by the medium size model is confirmed by the results appearing in figure 22. In this figure, plots similar to those previously shown in figures 19 through 21 are presented for the medium and small models at the same test Reynolds number - 0.6 million. Corrections for unequal Reynolds number are therefore unnecessary, and direct comparisons can be made. It will be observed from these direct comparisons that none of the conclusions previously arrived at from consideration of figure 21 is to any extent altered by the data in figure 22. In particular, the range of Mach numbers and angles of attack over which good agreement exists is the same in the one figure as it is in the other. Furthermore, it is evident that such differences as do occur lie predominantly in the same direction and are approximately of the same magnitude.

Interference on similar models.- From the results contained in figures 21 and 22, it can be stated that test data obtained in this wind tunnel for wing-body models similar to the one tested, having frontal projected areas 1/2 percent or less of the test-section cross-sectional area and span-to-tunnel-height ratios not greater than one-half may contain interference errors in C_L as large as about 5 percent, up to 8° angle of attack. For C_D the errors may be as large as 11 percent at 0° angle of attack, decreasing to about 6 percent at between 4° and 8° angles of attack. For C_m, errors as large as 13 percent may occur at supersonic speeds. It should be kept in mind that smaller errors for C_L and C_D could possibly be quoted had the strain-gage balances been of better accuracy.

Shock-Wave Attenuation From Pressure Measurements

The results of previous sections have shown indirectly the efficacy of the 6-percent-open walls in attenuating boundary-reflected disturbances.

Further and direct evidence of this property is shown in figure 23. This plot presents pressure surveys at supersonic Mach numbers measured at a time when the upstream ends of the two vertical side walls of the test section were protruded into the air stream. These protrusions formed crescent-shaped steps on the opposing sides of the tunnel, at the nozzle exit, which varied in height from 0 at the ends (which were in the tunnel corners) to 0.037 inch at the center on one side and 0.023 inch on the other. They resulted in the formation of a strong compression-expansion wave, apparent in the figure at all Mach numbers above 1.05. It is clearly seen that the strength of the reflections from this wave were considerably reduced farther downstream. Quantitative evaluation of the wave attenuating capabilities of the walls from these data is not possible, because no corresponding solid-wall data are available for comparison, and the measurement points were not frequent enough (2-inch intervals) to always detect the peak magnitudes of the compression waves. Yet is is worth noting that at 1.25 Mach number, the Mach number variations in the model test region are only about 10 percent that of the initial disturbance.

Pressure-Ratio Requirements

Figure 24 has been prepared to illustrate the power required by the Ames 2- by 2-foot transonic wind tunnel. Information has also been included to appraise the efficiency of the effuser, and to indicate the reduction in power made possible by use of the suction pump as a supplement to the effuser for removing air from the plenum chamber.

On figure 24 the static-pressure ratio between stations 1 and 2 (see fig. 1) has been plotted as a function of Mach number with the test section empty, and with a representative model at $1/4^{\circ}$, 8°, and 12° angles of attack. Two groups of such curves are presented - the first shows the pressure ratios required when all of the air removed from the plenum chamber leaves via the effuser; the second, the ratios when air is removed with both effuser and suction pump. The gross rate of air removal in both cases is approximately the same, the amount removed by the suction pump (shown by the dashed curve in fig. 24) having been adjusted so that the plenum-chamber pressure was the same as when only the effuser was used.

This figure shows that pressure ratios as high as 1.26 are required just to obtain a tunnel-empty Mach number of 1.4. To achieve this Mach number with a model installed, even higher ratios are necessary. The figure also shows that large reductions in pressure ratio are provided by the suction pump, although the amount of flow removed is as low as 1 to 1-1/2 percent of the tunnel mass flow. This result, of course, implies both that the effuser efficiency is low and that sizable power savings are provided by the suction pump.

Figure 25 shows values of effuser efficiency plotted versus test-section Mach number, and figure 26 the net power saved as a proportion of total power input to the main drive. As used here, effuser efficiency is defined as the ratio of power required to deliver air from the plenum chamber to the main compressor inlet with zero loss to the power actually required. The power actually required is equal to the difference in main-drive power required when using the effuser alone and when using both the effuser and suction pump. Inspection of these figures indicates that the effuser efficiency is low, varying roughly from 15 to 20 percent over the Mach number range 1.1 to 1.3. The power saving available through use of the suction pump is correspondingly large, averaging somewhat more than 15 percent of the main power without suction and amounting to between 300 and 400 horsepower per atmosphere of settling-chamber pressure.

SUMMARY OF RESULTS

The Ames 2- by 2-foot transonic wind tunnel has been described as a research facility in which the Mach number can be varied continuously from low subsonic values up to 1.4.

From Mach number surveys in the empty wind tunnel it has been shown that the Mach number variation is ±0.003 over a 20-inch length up to 1.35 Mach number, and ±0.005 over an 18-inch length at 1.40 Mach number.

For test models having frontal projected areas 1.15 and 0.51 percent of the tunnel cross-sectional area, large reductions in wall interference were attained with 6-percent open-area perforated walls, as compared to practically solid walls, perforated in the corners to prevent choking. For the 0.51-percent-blockage model, in the supersonic speed range, these reductions amounted to as much as 80 percent for drag coefficient.

From these tests it is concluded that the wall interference is small for a model having a projected frontal area of 1/2 percent of the cross-sectional area of the test section and a wing-span-to-tunnel-height ratio of one-half. For models of this size no empirical corrections to test data are at present considered necessary.

Auxiliary suction has been shown to be an effective means of reducing the main compressor pressure-ratio requirements and over-all power consumption. The use of between 1 and 1-1/2 percent mass removal can result in about a 15-percent reduction in main-drive power.

Ames Aeronautical Laboratory
    National Advisory Committee for Aeronautics
        Moffett Field, Calif., Sept. 21, 1955

REFERENCES

1. Wright, Ray H., and Ward, Vernon G.: NACA Transonic Wind-Tunnel Test Sections. NACA RM L8J06, 1948.

2. Bird, K. D., and Martin, J. F.: Results of Calibrations and Various Model Configuration Tests in the 4-Foot Transonic Wind Tunnel. Rep. No. AD-844-W-3, Cornell Aero. Lab., Inc., Buffalo, Aug. 1953.

3. Allen, H. Julian, and Spiegel, Joseph M.: Transonic Wind Tunnel Development at the NACA Ames Aeronautical Laboratory. IAS Preprint 474, June 24, 1954.

4. Pindzola, Michael: Shock and Expansion Wave Cancellation Studies in a Two-Dimensional Porous Wall Transonic Tunnel. Rep. R-25473-5, United Aircraft Corp., East Hartford, Conn. Res. Dept., Sept. 1951.

5. Goethert, B. H.: Flow Establishment and Wall Interference in Transonic Wind Tunnels. AEDC-TR-54-44, June 1954.

6. Holder, D. W., and North, R. J.: A Colour-Schlieren Apparatus. ARC, Fluid Motion Sub-Comm. 12,856 (FM 1405), Jan. 1950.

7. Westkaemper, J. C.: Supersonic Flow Visualization in Color. Memo. 67, Ordnance Aerophysics Laboratory, Daingerfield, Texas.

8. Goethert, Bernhard H.: Influence of Plenum-Chamber Suction and Wall Convergence on the Mach Number Distribution in Partially Open Test Sections of Wind Tunnels at Subsonic and Supersonic Speeds. AEDC-TR-54-42, Apr. 1955.

9. Tunnell, Phillips J.: An Investigation of Sting-Support Interference on Base Pressure and Forebody Chord Force at Mach Numbers From 0.60 to 1.30. NACA RM A54K16a, 1955.
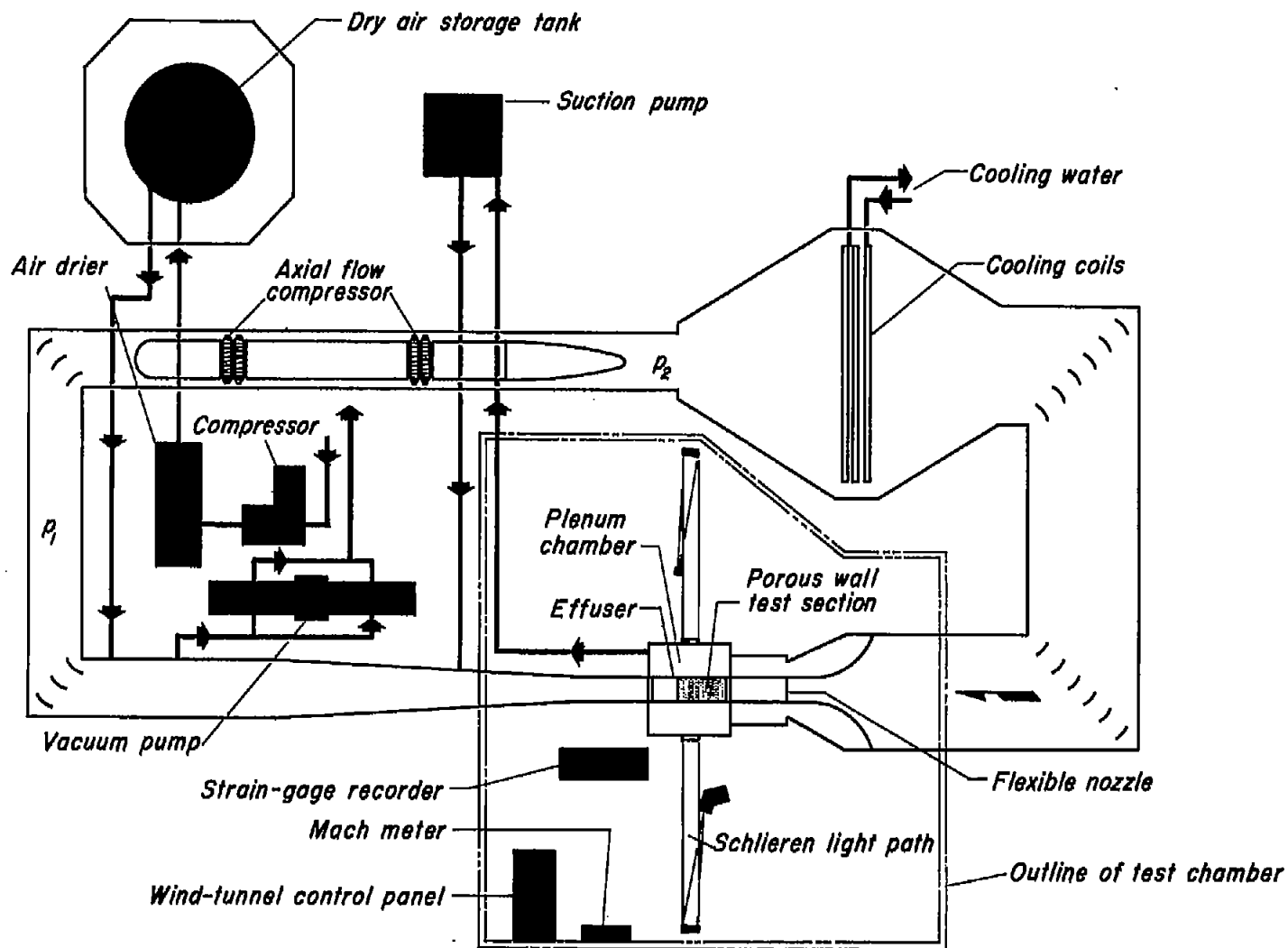
Figure I.— Schematic drawing of the 2- by 2- foot transonic wind tunnel showing tunnel layout with auxiliary equipment.

Perforated wall

① Flexible nozzle   ④ Effuser
② Plenum chamber   ⑤ Model support
③ Mobile pressure cylinder   ⑥ Diffuser
        ⑦ Schlieren light path
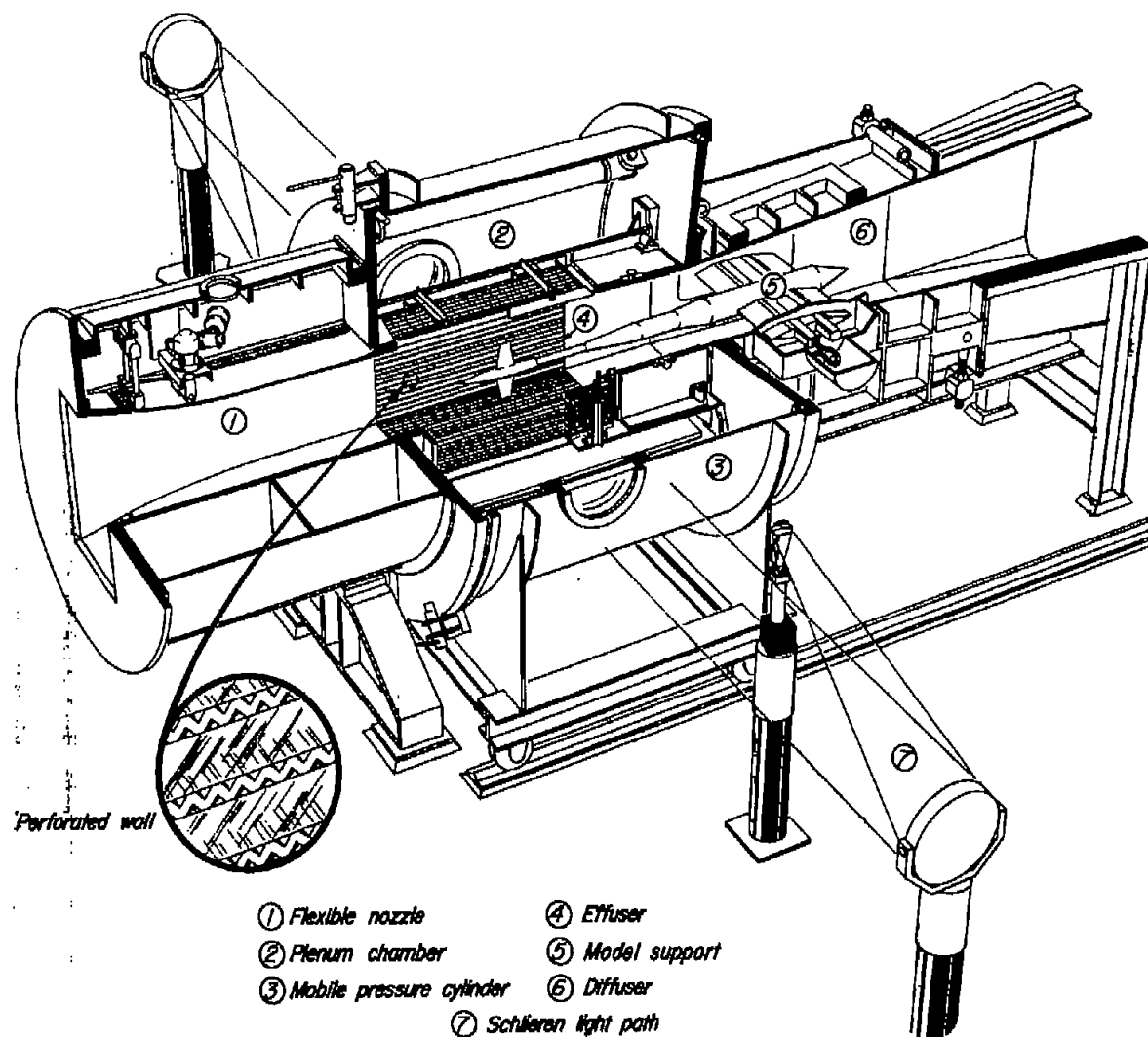
Figure 2.- Sectional view of the high-speed region of the 2-by 2-foot transonic wind tunnel.
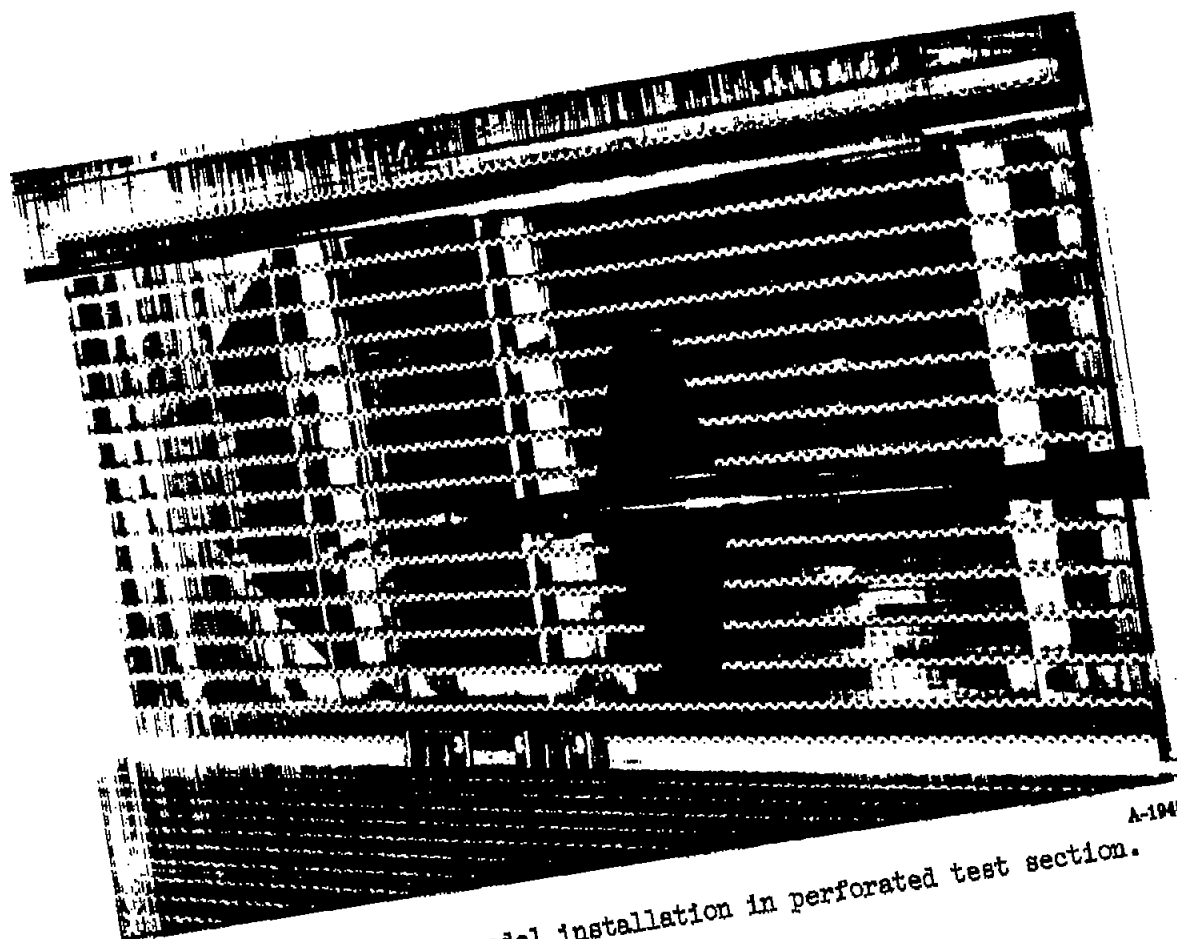
A-19451

Figure 3.- Typical model installation in perforated test section.
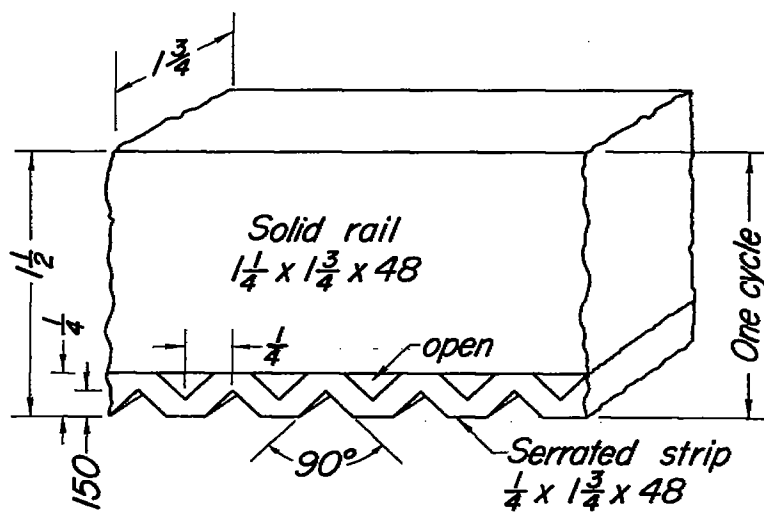
(a) Perforated-wall geometry, 6-percent open area.
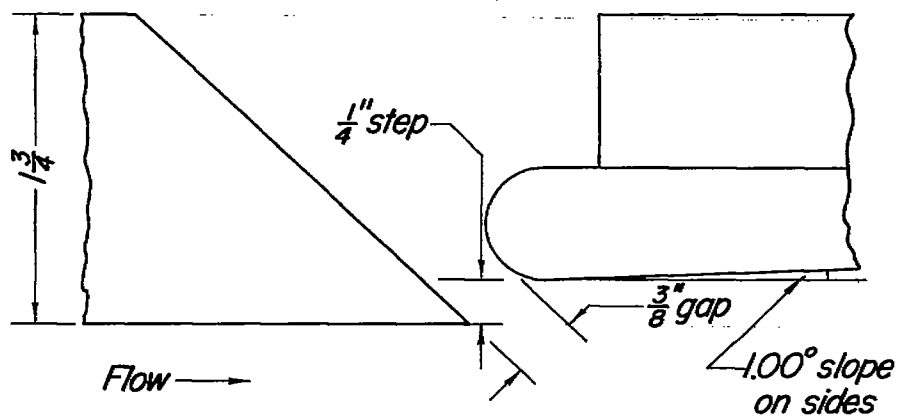
(b) Effuser detail, (location ④ figure 2).

Figure 4.- Geometry of test-section porosity and effuser
for the 2-by 2-foot transonic wind tunnel.
(All dimensions in inches)

Section CC

Section BB

Section AA

.001

Recess for sting

Model supported by gaged
compression fit on conical section

End view

Gage location	Component Indicated
①	Front normal force
②	Rear normal force
③	Front side force
④	Rear side force
⑤	Rolling moment
⑥	Chord force

.70 .45

Plan view

Drag link to be inserted at section BB.

Direction of Force Application

(a) Normal force − z Direction
(b) Side force − y Direction
(c) Chord force − x Axis
(d) Rolling moment − Rotation about
                       x axis

Figure 5.− Sketch of the six-component flexure balance used in the 2-by 2-foot transonic wind tunnel.

(All dimensions in inches)
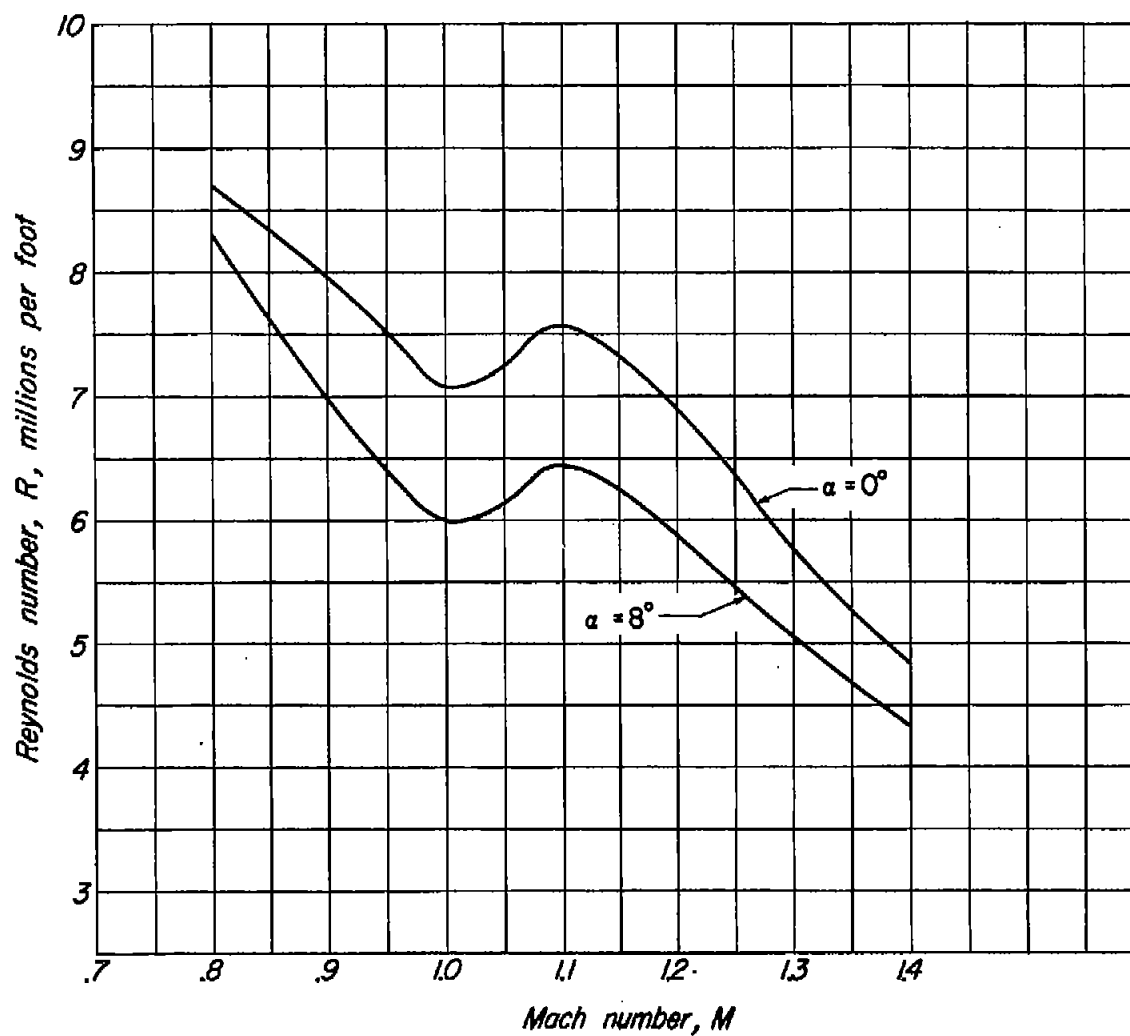
Figure 6.- Variation of the maximum Reynolds number with Mach number for the 2-by 2-foot transonic wind tunnel.
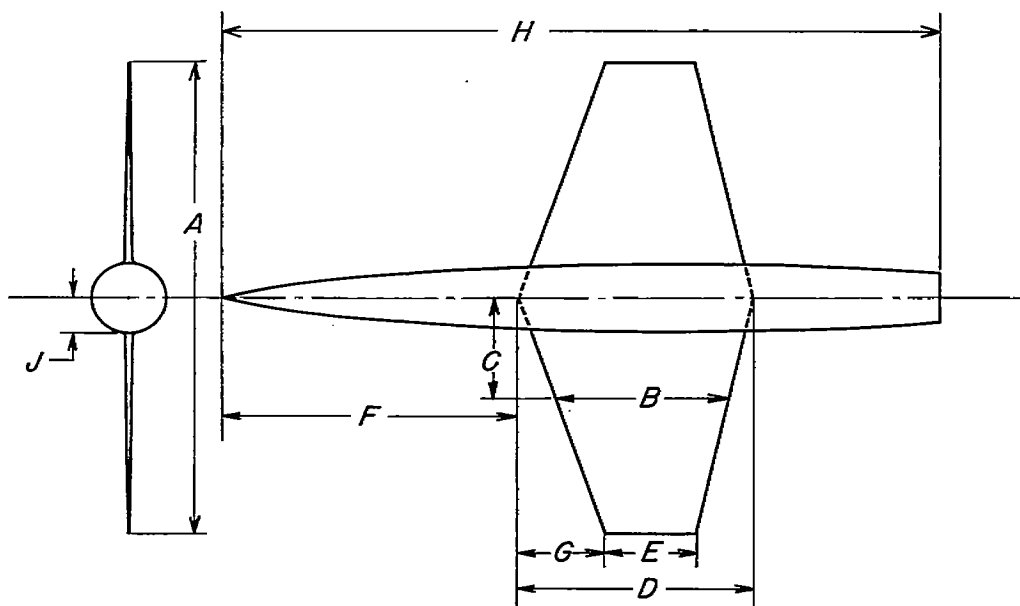
GEOMETRY OF THE MODELS

	Figure symbol	Small model	Medium model	Large model
Span, in.	A	4.690	10.946	16.418
Area, sq in.		7.126	38.808	87.311
$\bar{c}$, in.	B	1.618	3.776	5.664
Span $\bar{c}$ location, in.	C	1.002	2.335	3.500
Root chord, in.	D	2.188	5.106	7.659
Tip chord, in.	E	.851	1.985	2.977
Body nose to wing apex, in.	F	2.783	6.490	9.727
Wing apex to wing tip L.E.,in.	G	.812	1.895	2.842
Wing incidence, deg		0	0	0
Body length,(theoretical),in.	l	8.500	19.833	29.750
Body length, (actual),in.	H	6.705	15.644	23.467
Maximum body radius, r_o,in.	J	.340	.794	1.109
Model blockage area,percent tunnel cross section		.09	.51	1.15
Base area of body, sq in.		.197	1.075	2.420
Body radius, r, in. $r=r_o\left[1-\left(1-\frac{2(body\ station)}{body\ length,\ l}\right)^2\right]^{3/4}$				

Figure 7.- Geometric characteristics for the small, medium, and large test models
having 3 - percent- thick biconvex wing sections, aspect ratio = 3.09, taper
ratio = 0.389, sweep of leading edge =19.10°, and sweep of $\frac{c}{4}$ =11.5°.

(a) M = 0.80 to M = 1.00
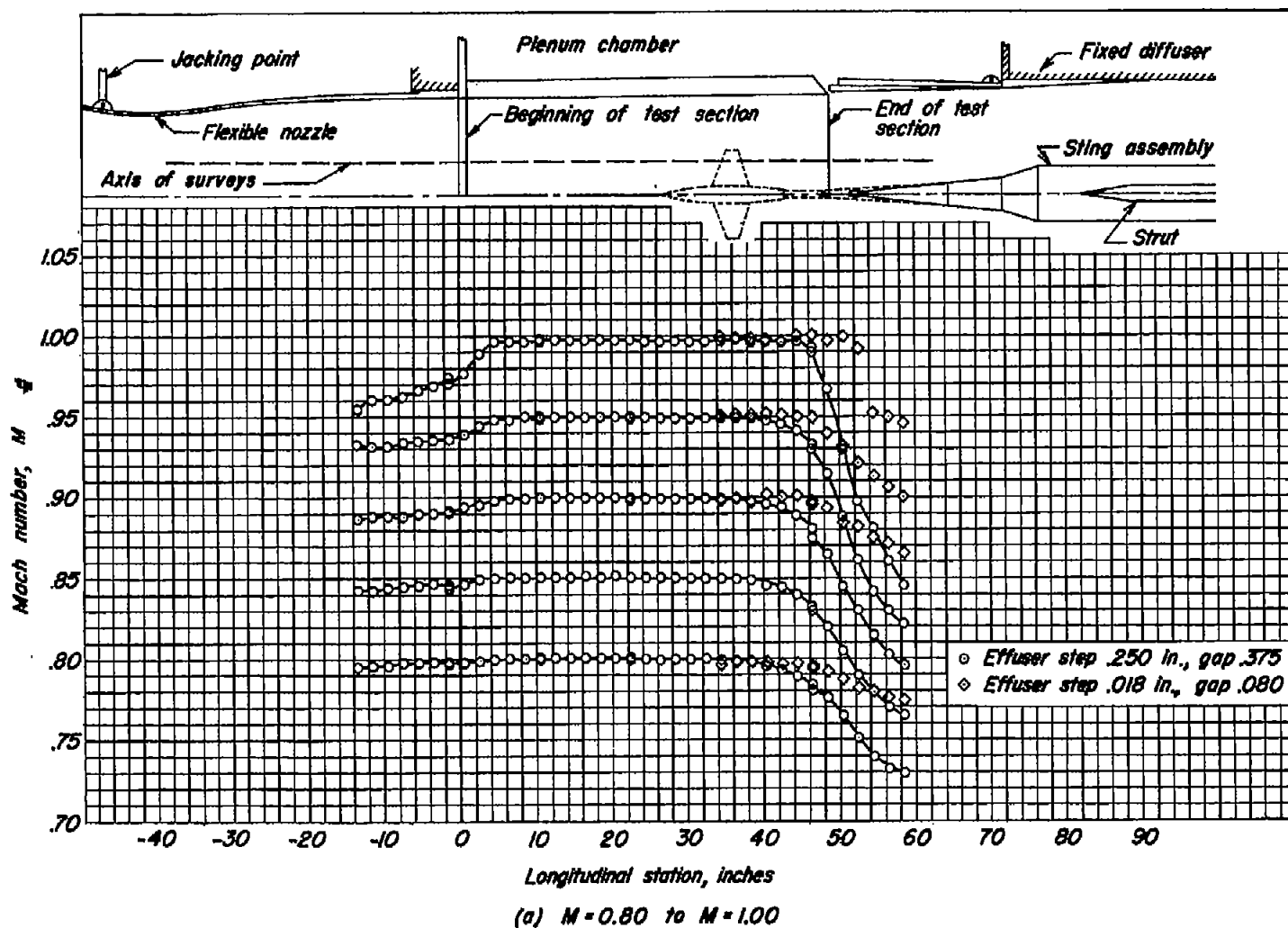
Figure 8.- Mach number distribution as obtained by axial survey on the vertical center line 4 inches above horizontal center line. (Tunnel empty)
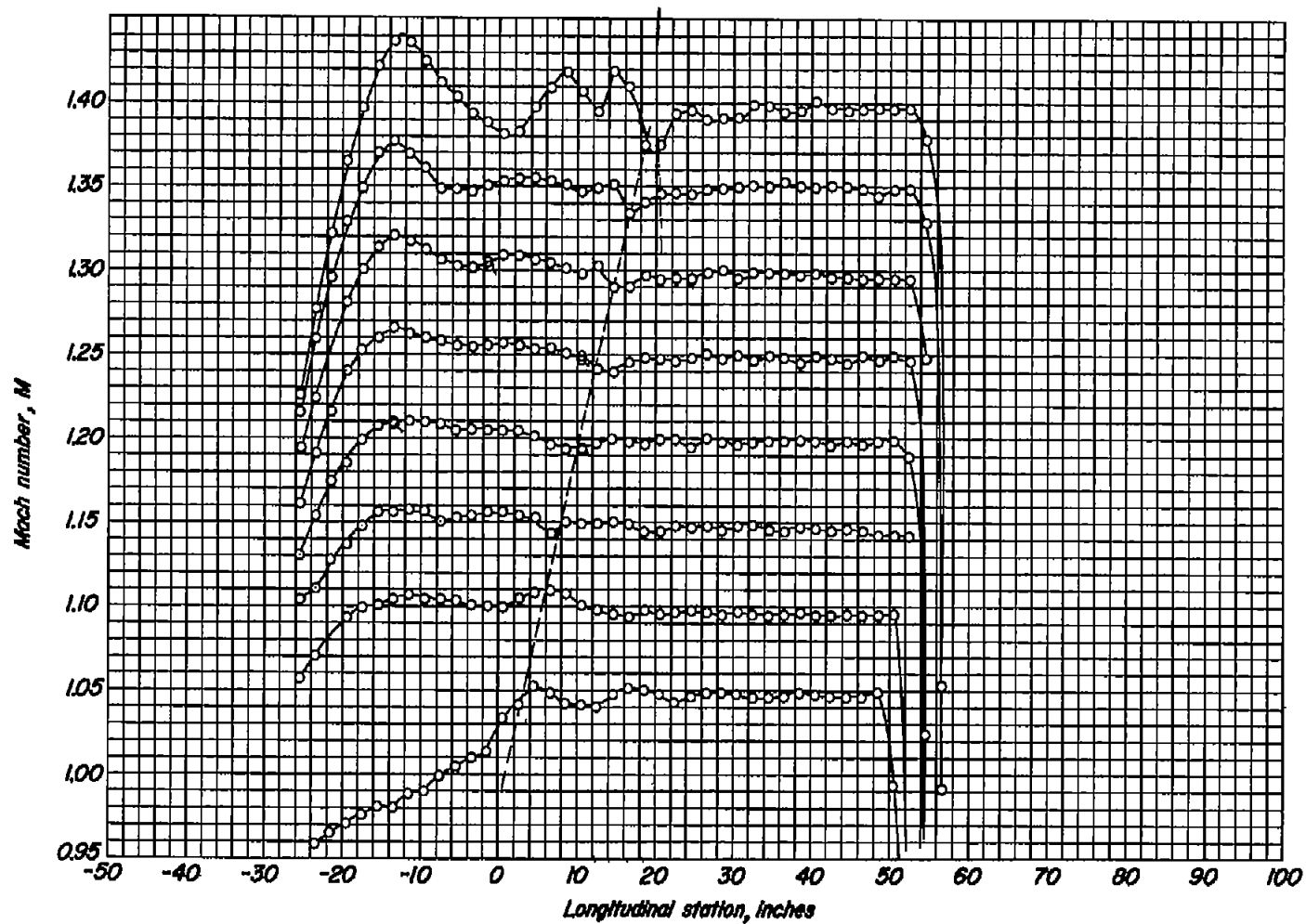
(b) M = 1.05 to 1.40

Figure 8.- Concluded.
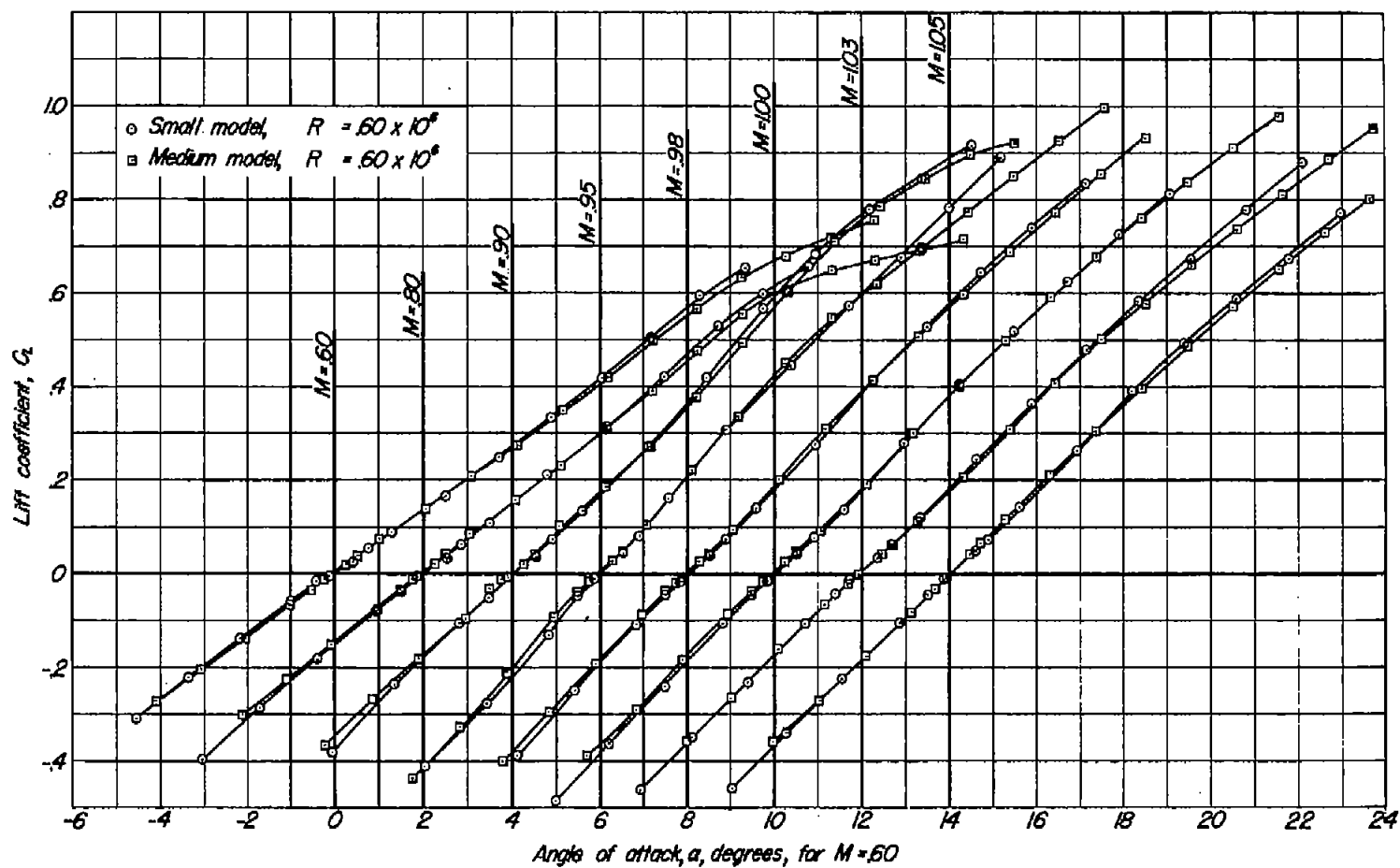
(a) M=0.60 to M=1.05

Figure 9.-Variation of lift coefficient with angle of attack at constant Mach numbers for comparison of small model to medium model at R =0.60 x 10⁶; 6-percent-open walls.

(b) M = 1.08 to M = 1.30

Figure 9.- Concluded.

(a) M = 0.60 to M = 1.05
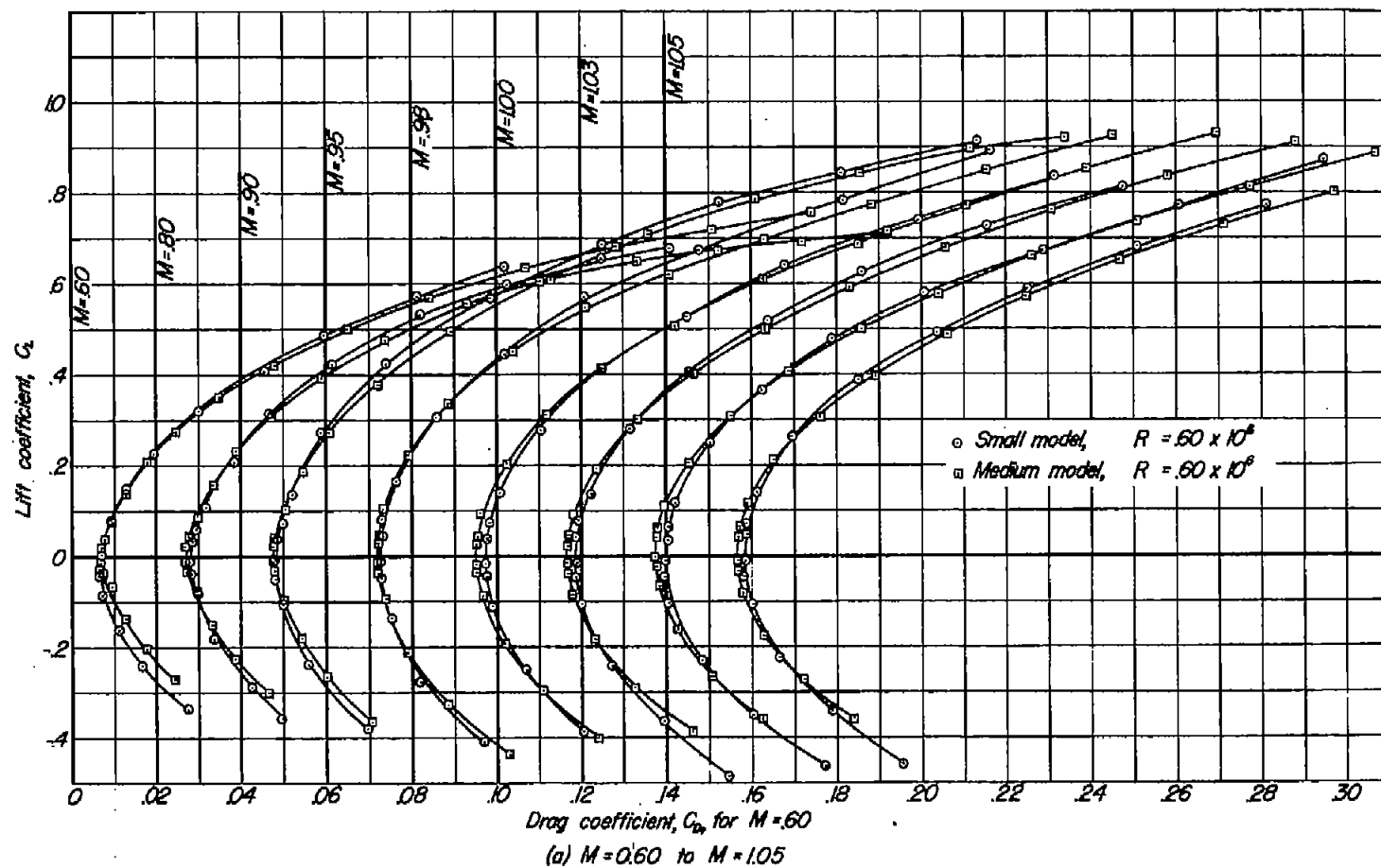
Figure 10.- Variation of lift coefficient with drag coefficient at constant Mach numbers for comparison of small model to medium model at R = 0.60 x 10⁶; 6-percent-open walls.

Lift coefficient, C_L

Drag coefficient, C_D, for M=1.08

(b) M=1.08 to M=1.30

Figure 10.- Concluded.

○ Small model, R = .60 x 10⁶

▢ Medium model, R = .60 x 10⁶

Pitching-moment coefficient, C_m

(a) $M = 0.60$ to $M = 1.05$
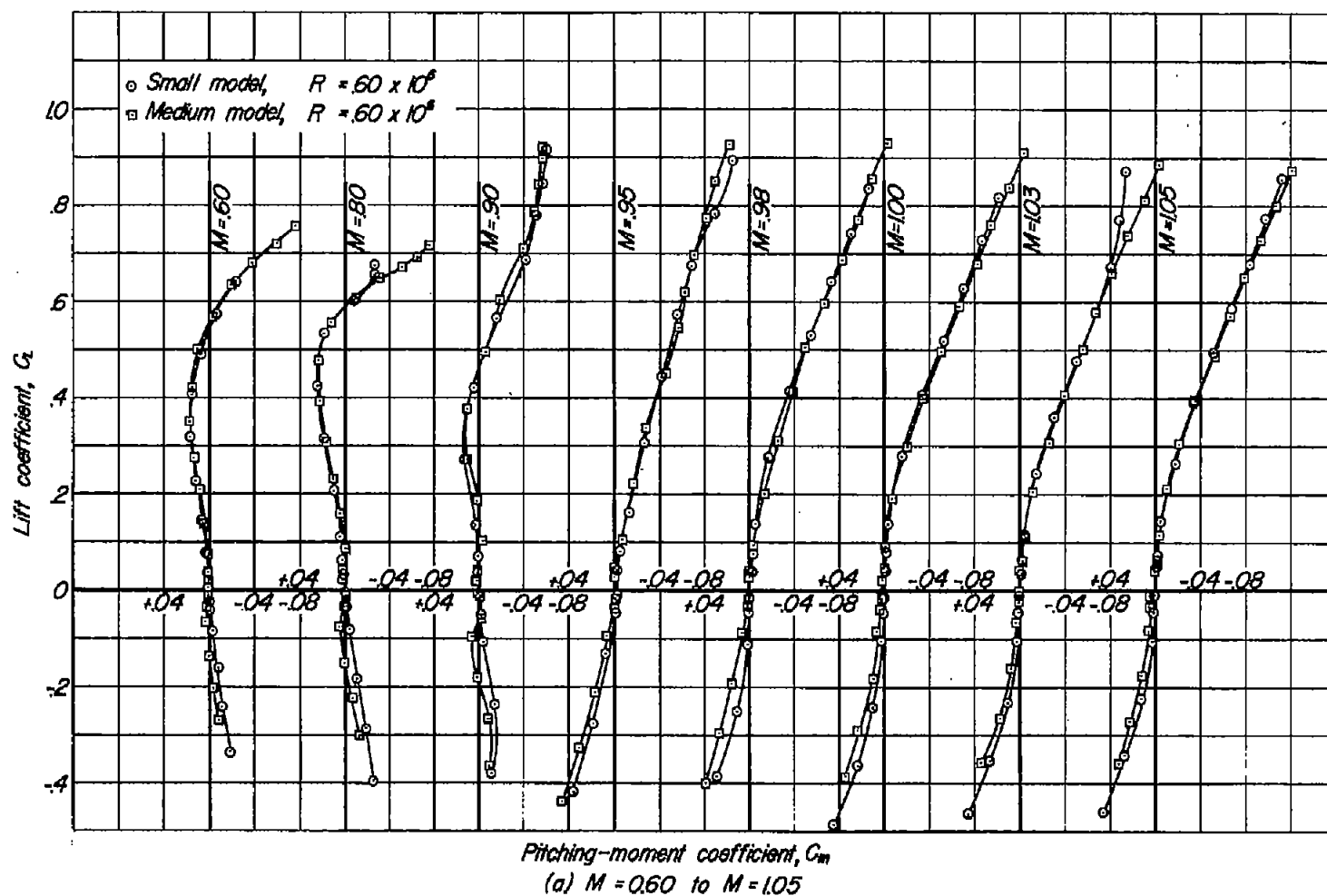
Figure 11.- Variation of lift coefficient with pitching-moment coefficient at constant Mach numbers for comparison of small model to medium model at $R = 0.60 \times 10^6$; 6-percent-open walls.

Pitching-moment coefficient, C_m

(b) M=1.08 to M=1.30

Figure II.-Concluded.
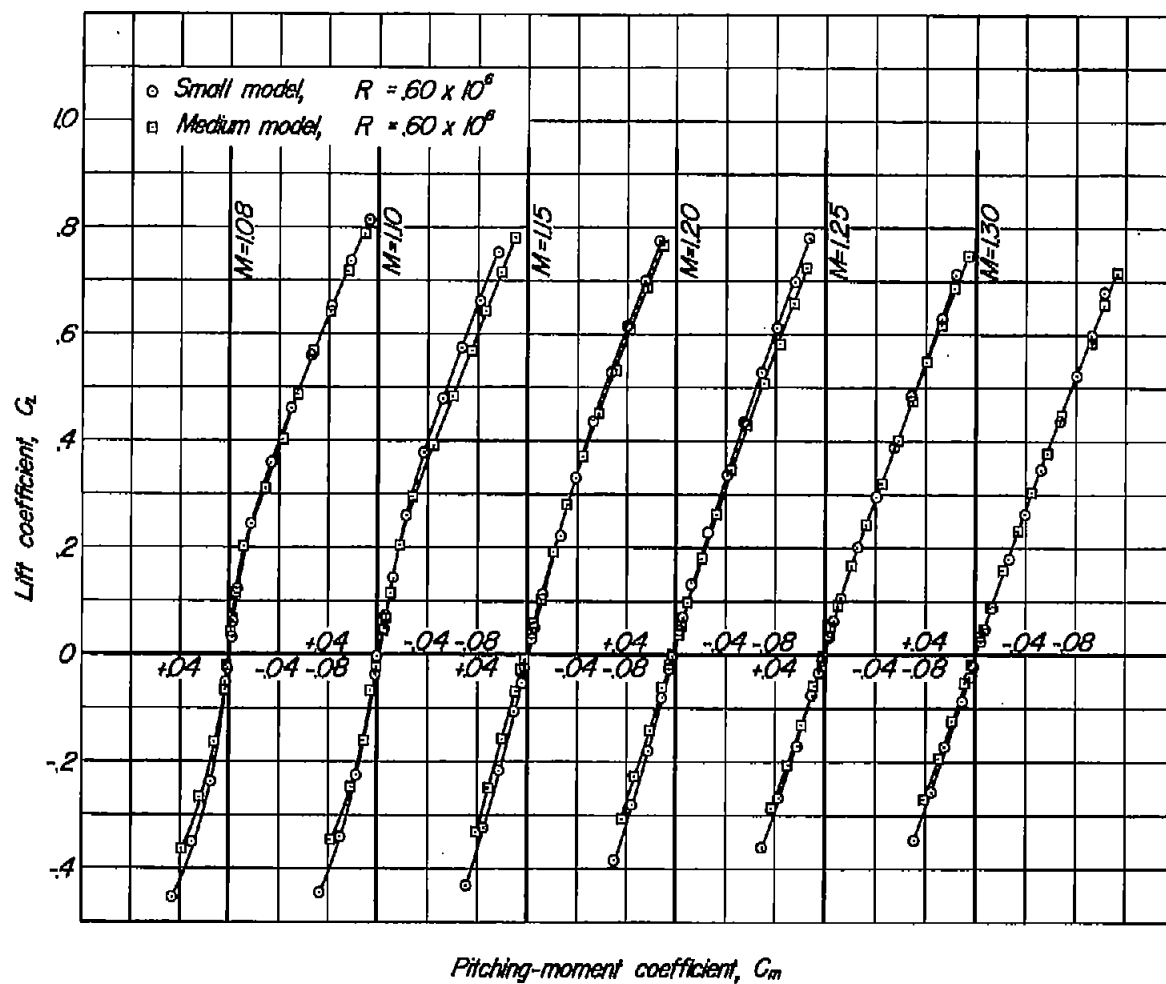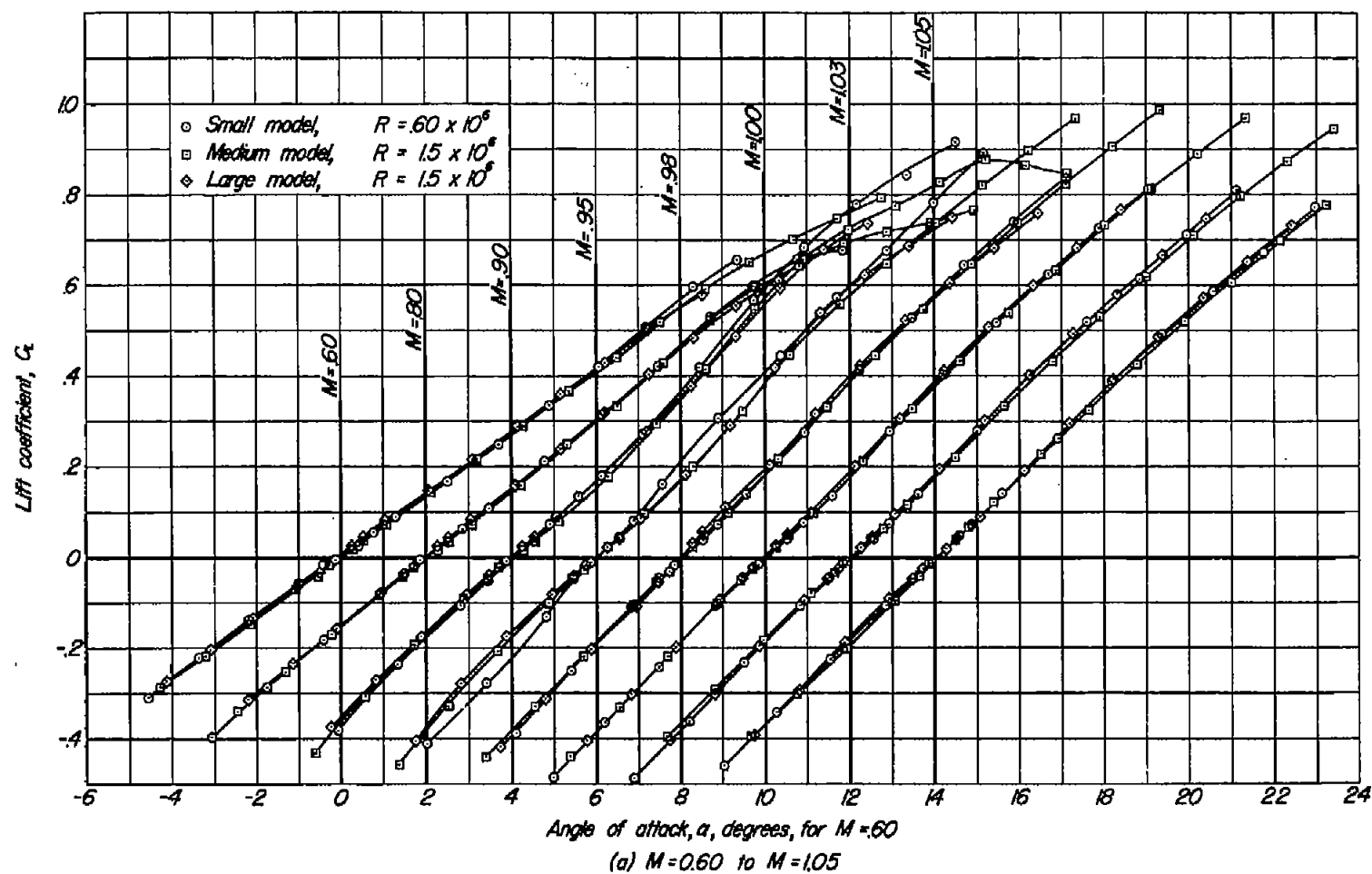
(a) M = 0.60 to M = 1.05

Figure 12.- Variation of lift coefficient with angle of attack at constant Mach numbers; 6-percent-open walls.

Angle of attack, α, degrees, for M =1.08
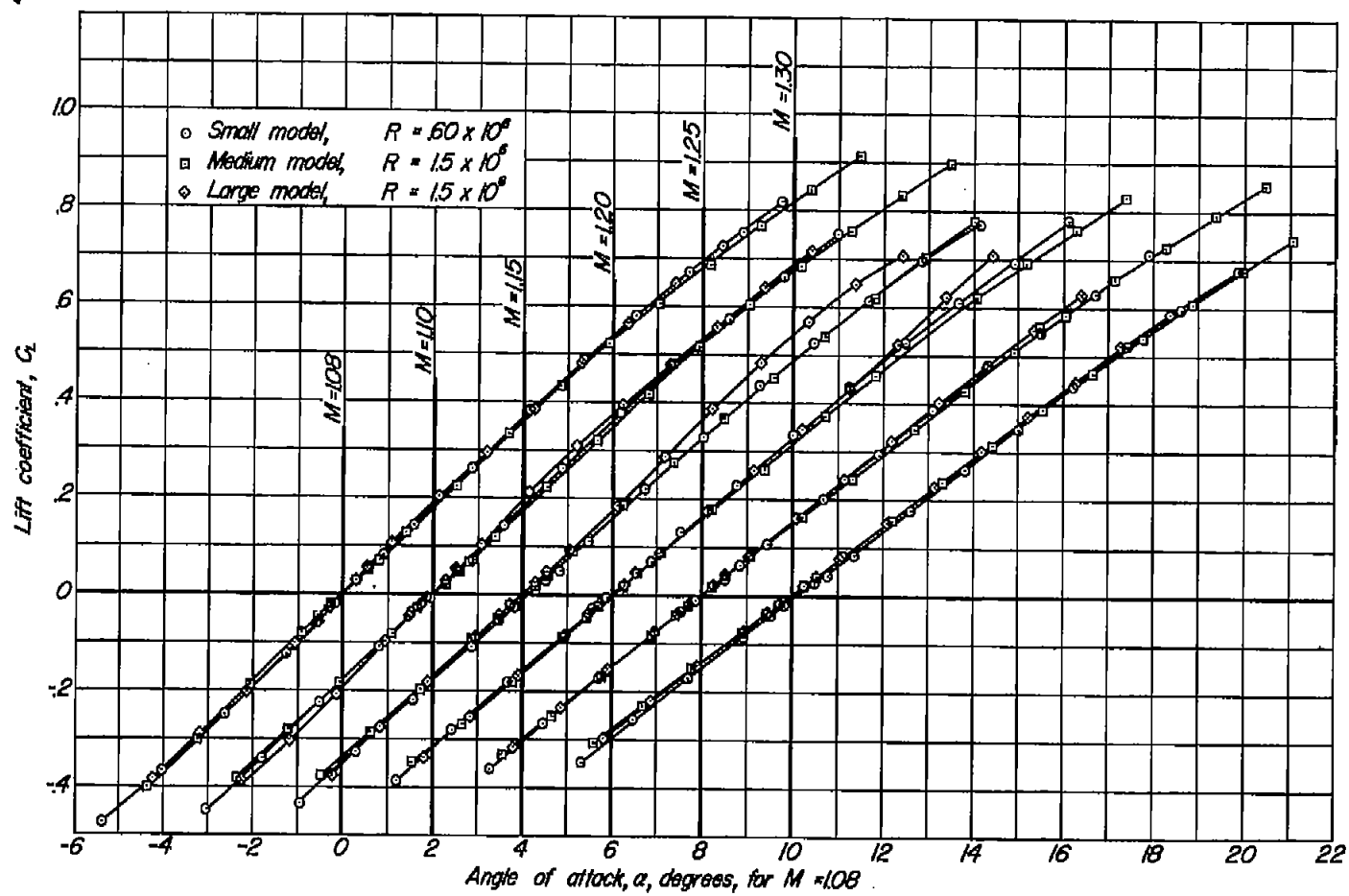
(b) M =1.08 to M=1.30

Figure 12.- Concluded.
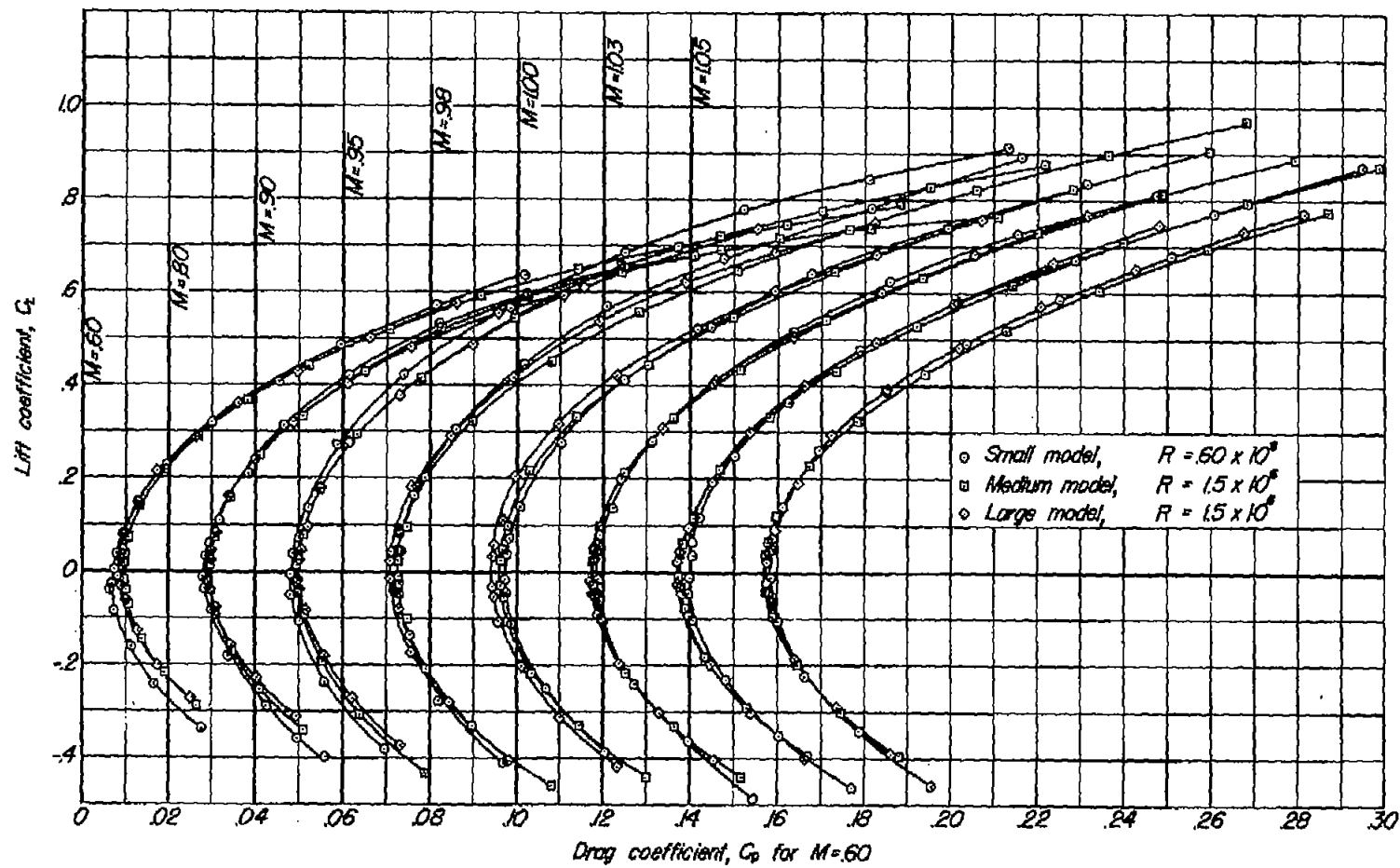
Figure 13.- Variation of lift coefficient with drag coefficient at constant Mach numbers; 6-percent-open walls.

(a) M = 0.60 to M = 1.05
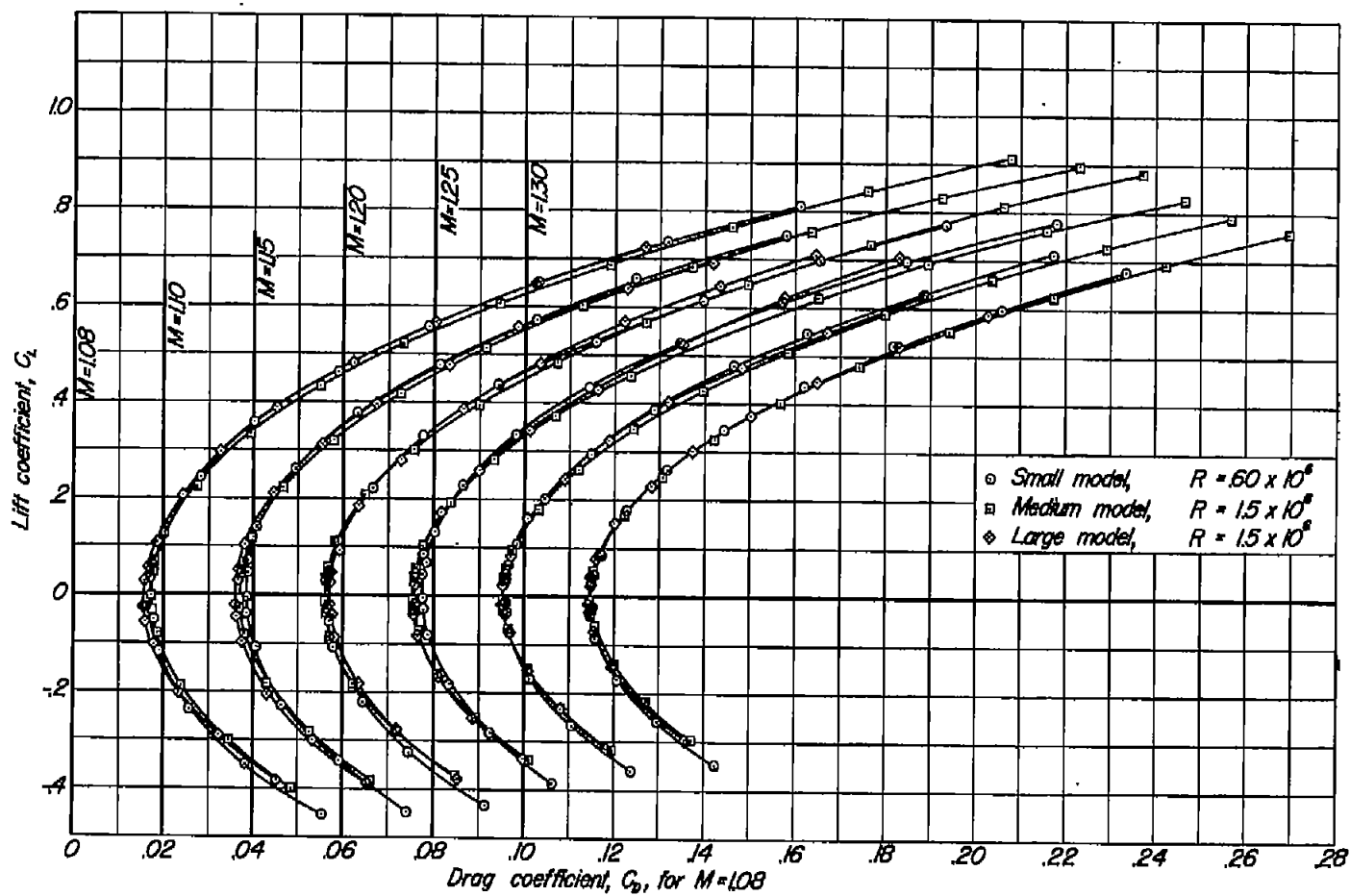
(b) M=1.08 to M=1.30

Figure 13.- Concluded.

Pitching—moment coefficient, C_m

(a) M = 0.60 to M = 1.05
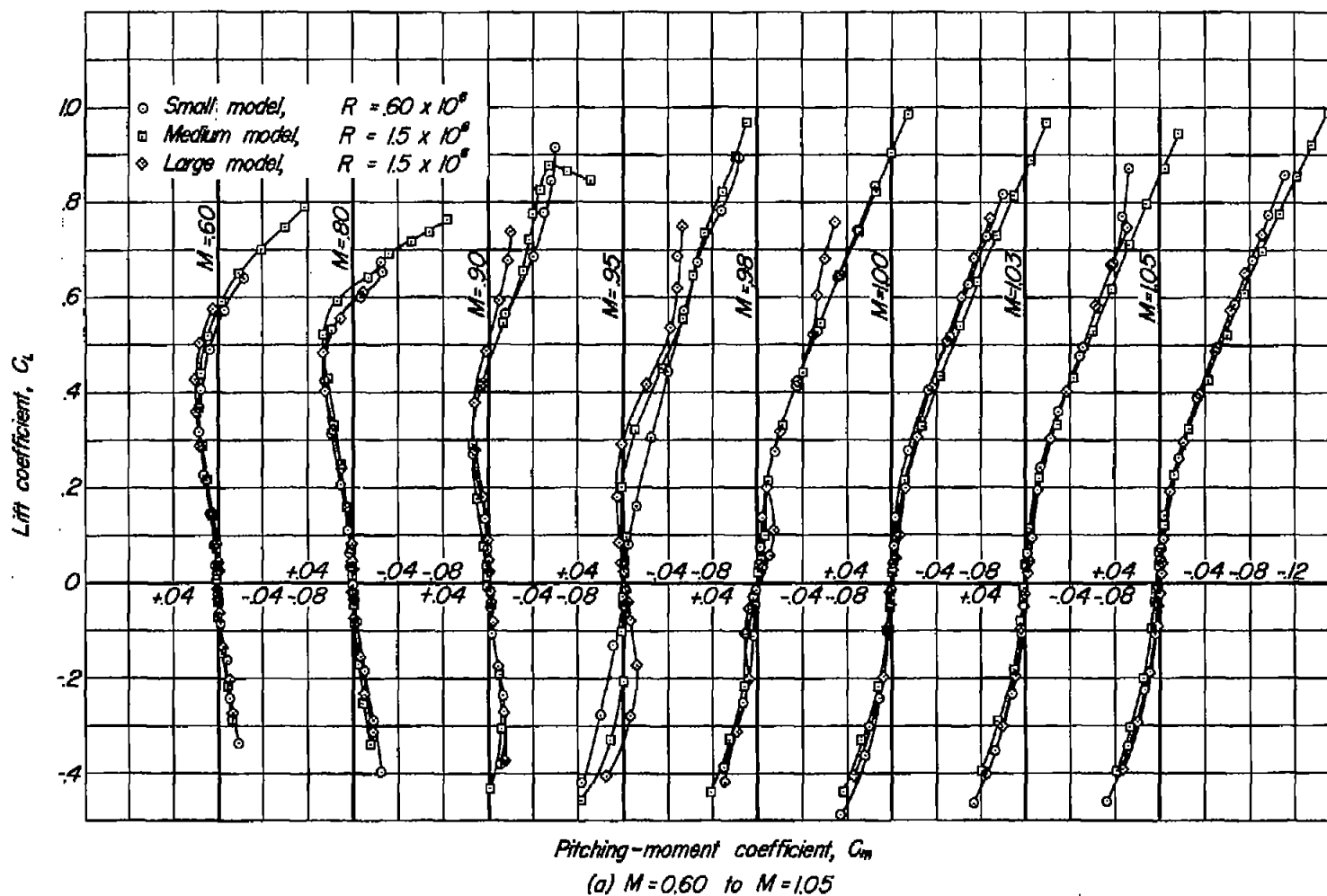
Figure 14.- Variation of lift coefficient with pitching—moment coefficient at constant Mach numbers; 6-percent-open walls.
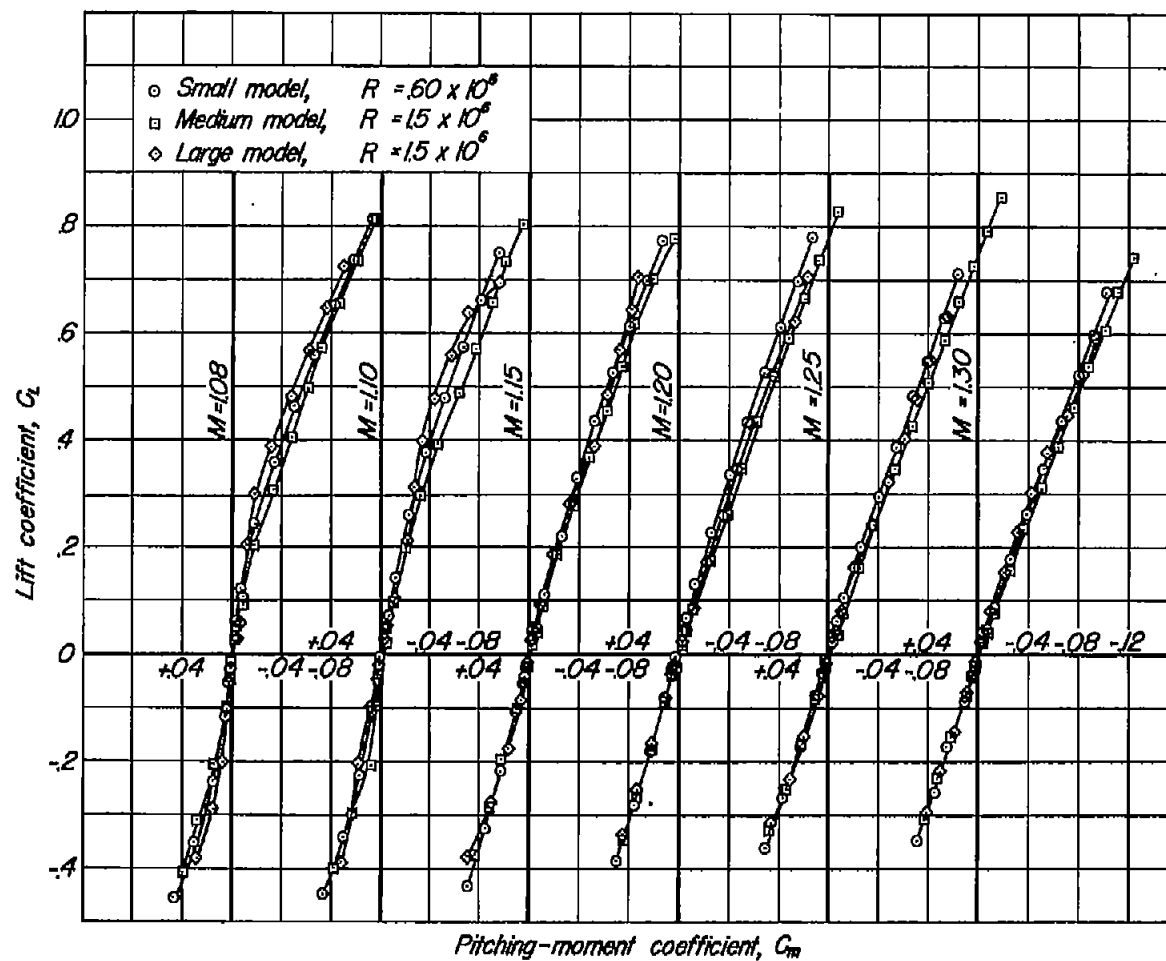
(b) M = 1.08 to M = 1.30

Figure 14.- Concluded.
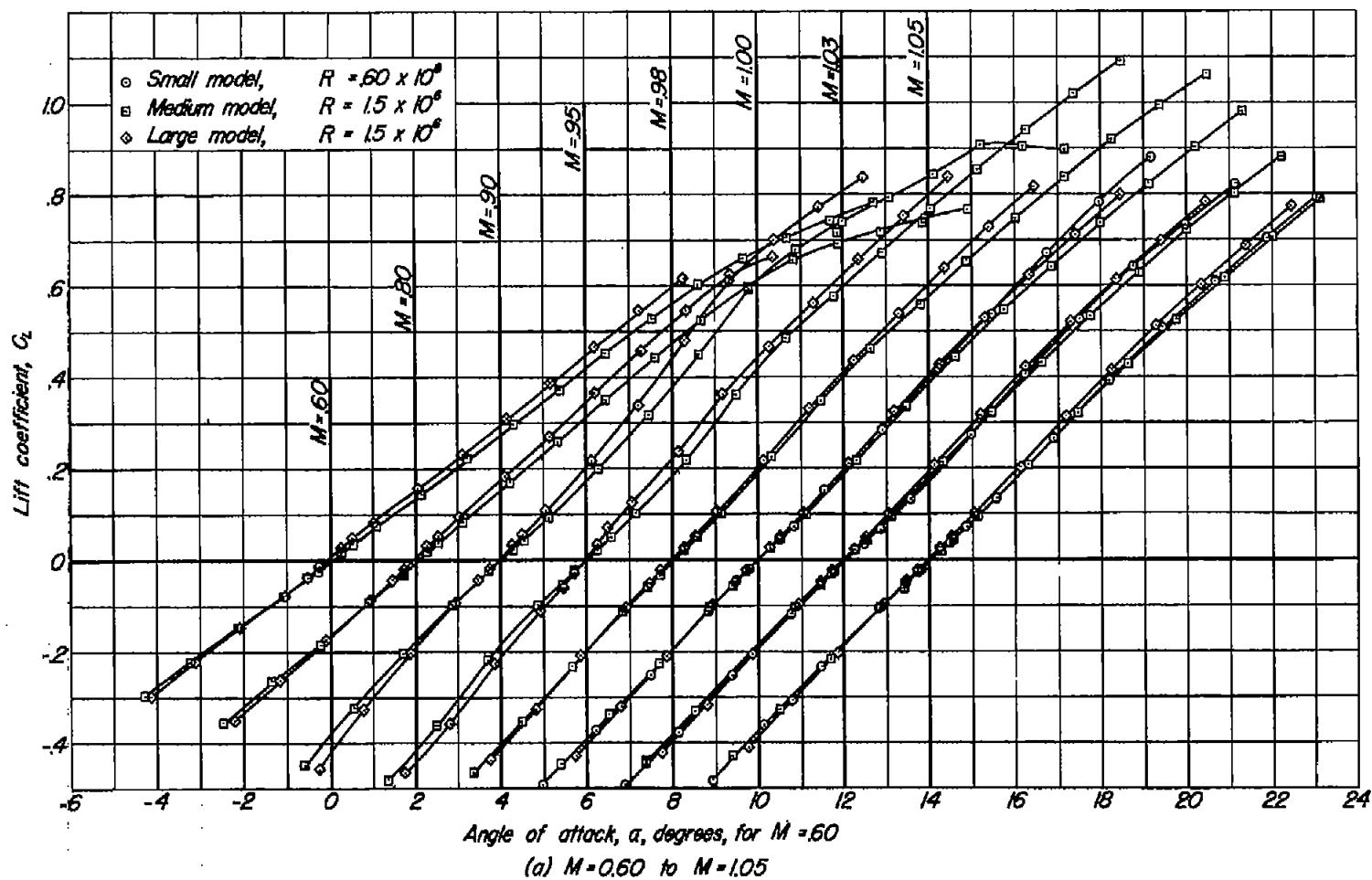
Figure 15.- Variation of lift coefficient with angle of attack at constant Mach numbers; quasi-solid walls.

(a) M = 0.60 to M = 1.05

Angle of attack, α, degrees, for M = .60

Lift coefficient, C_L

Small model,	$R = .60 \times 10^6$
Medium model,	$R = 1.5 \times 10^6$
Large model,	$R = 1.5 \times 10^6$
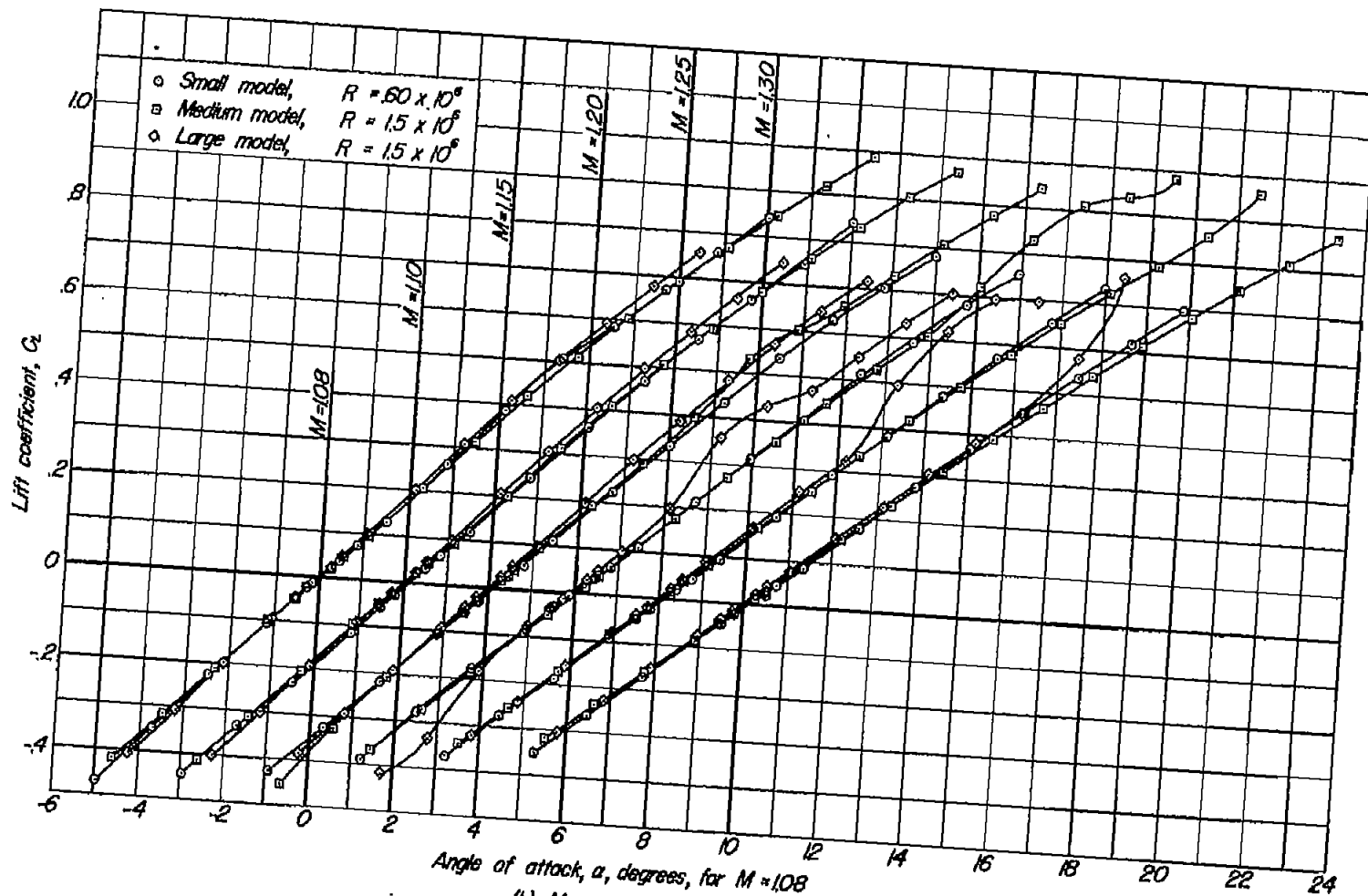
Figure 15.- Concluded.
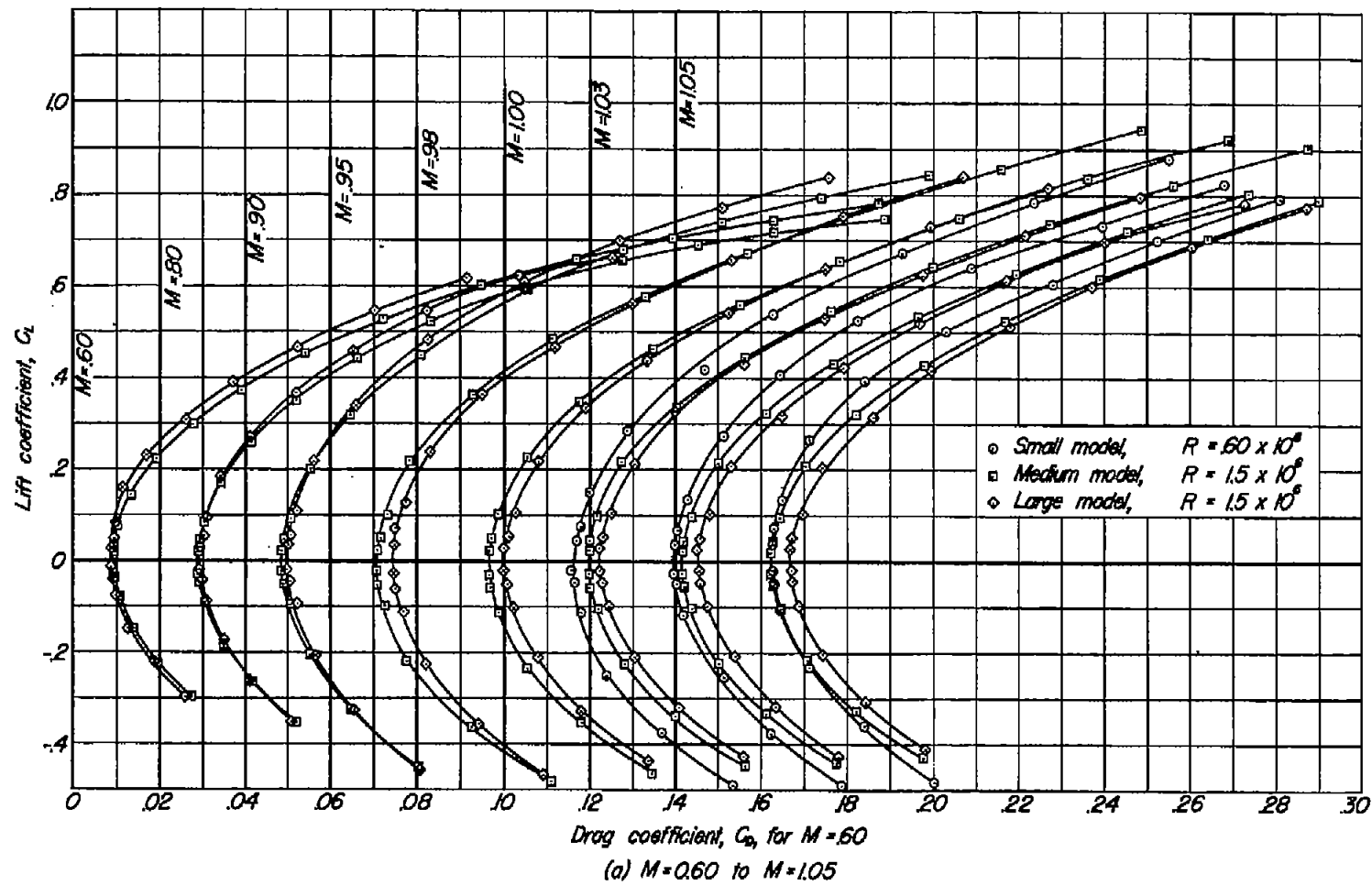
Figure 16.- Variation of lift coefficient with drag coefficient at constant Mach numbers; quasi-solid walls.

(a) M = 0.60 to M = 1.05

Drag coefficient, C_D, for M = .60

Lift coefficient, C_L

⊙ Small model,	R = .60 x 10⁶	
◻ Medium model,	R = 1.5 x 10⁶	
◇ Large model,	R = 1.5 x 10⁶	
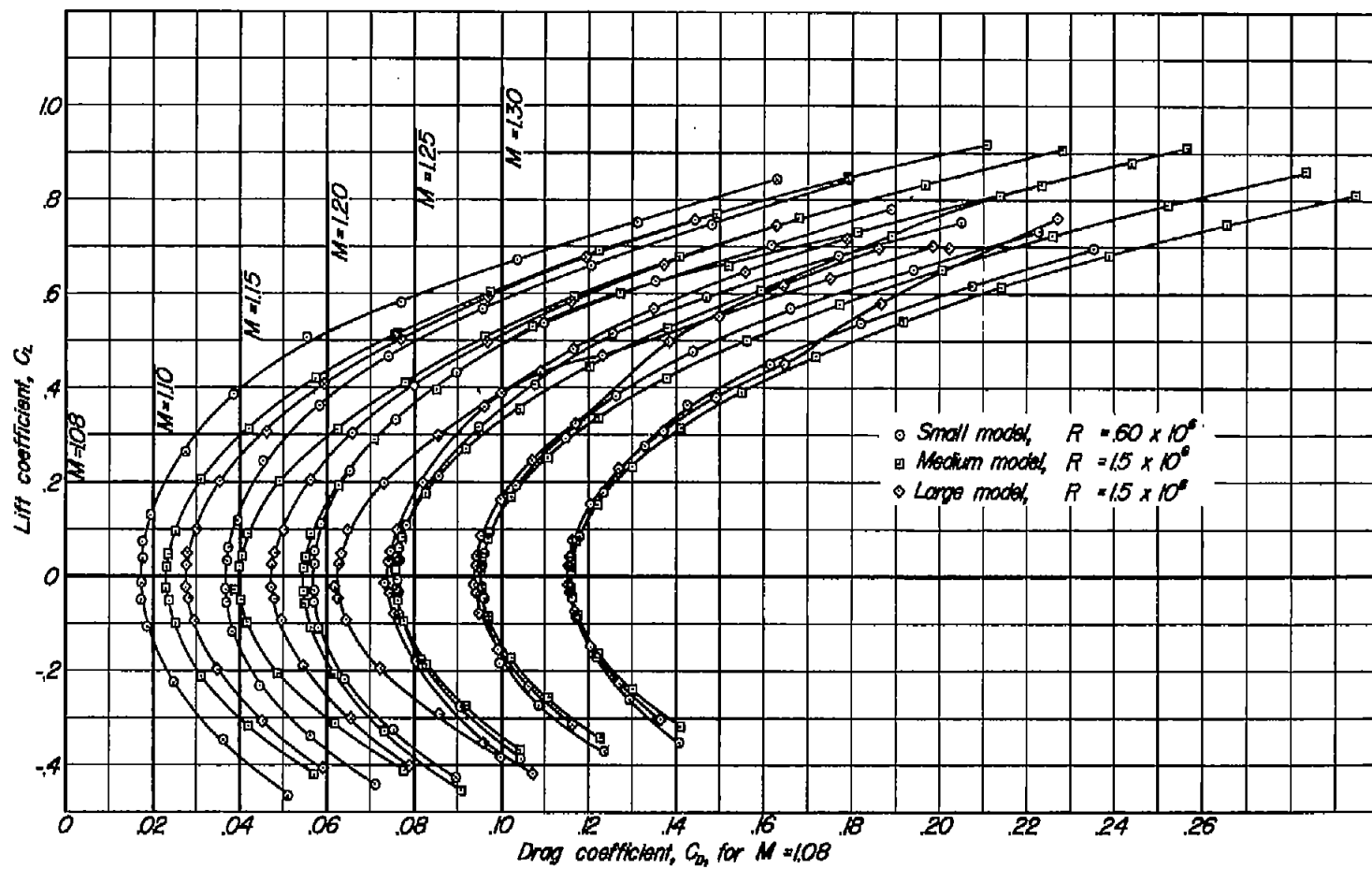
(b) M =1.08 to M =1.30

Figure 16.- Concluded.

Pitching-moment coefficient, C_m

(a) M = 0.60 to M = 1.05
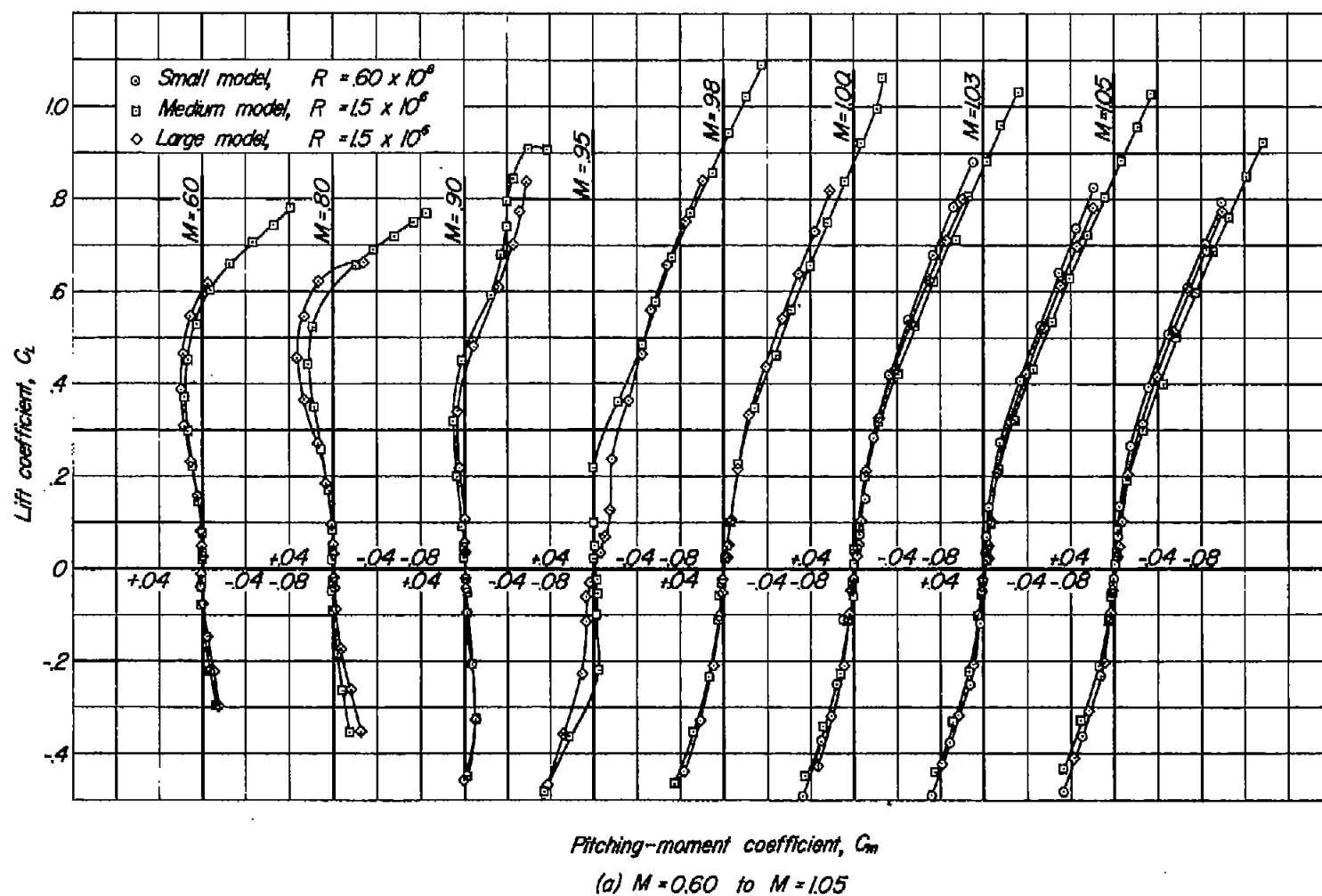
Figure 17.-Variation of lift coefficient with pitching-moment coefficient at constant Mach numbers; quasi-solid walls.
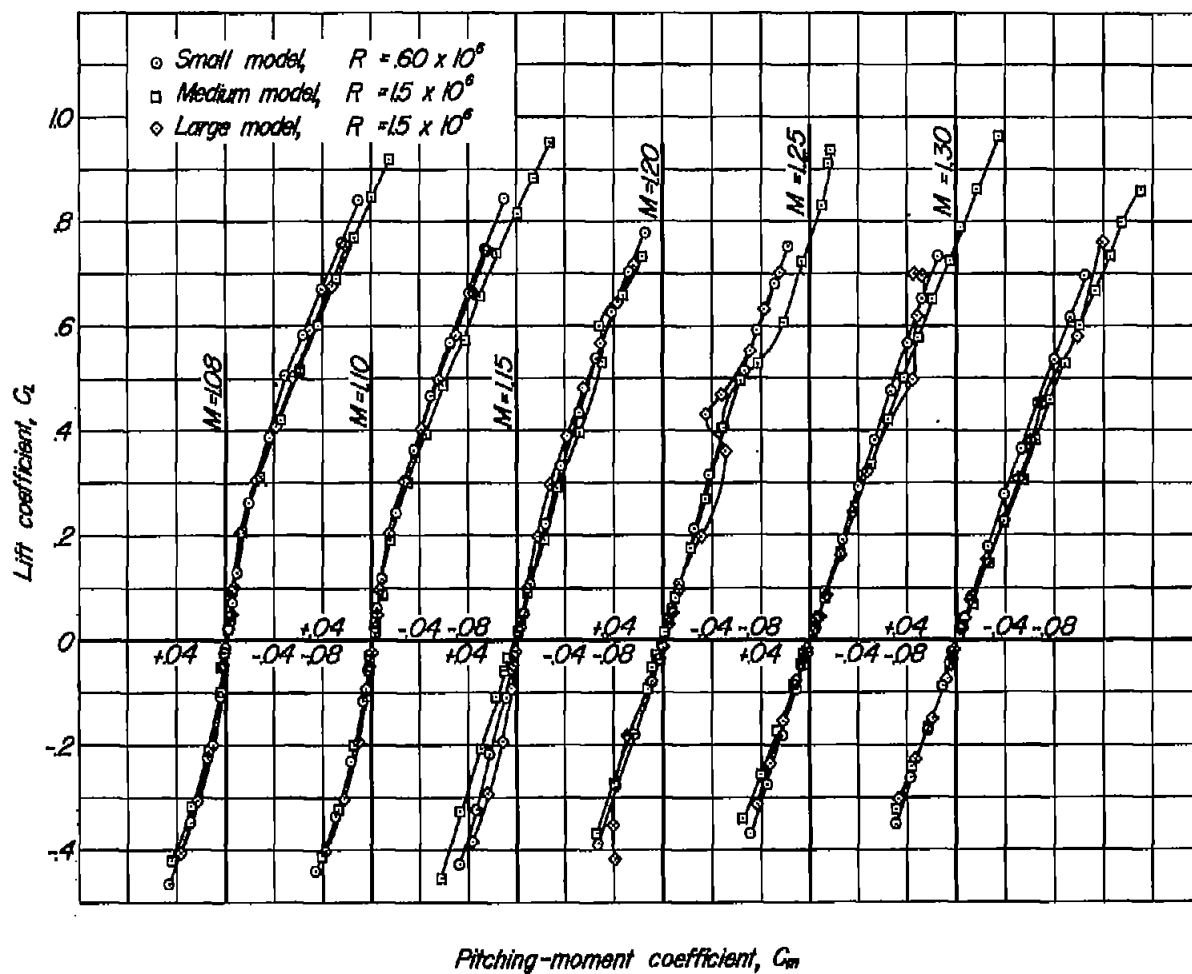
Pitching-moment coefficient, C_m

(b) M =1.08 to M =1.30

Figure 17.-Concluded.
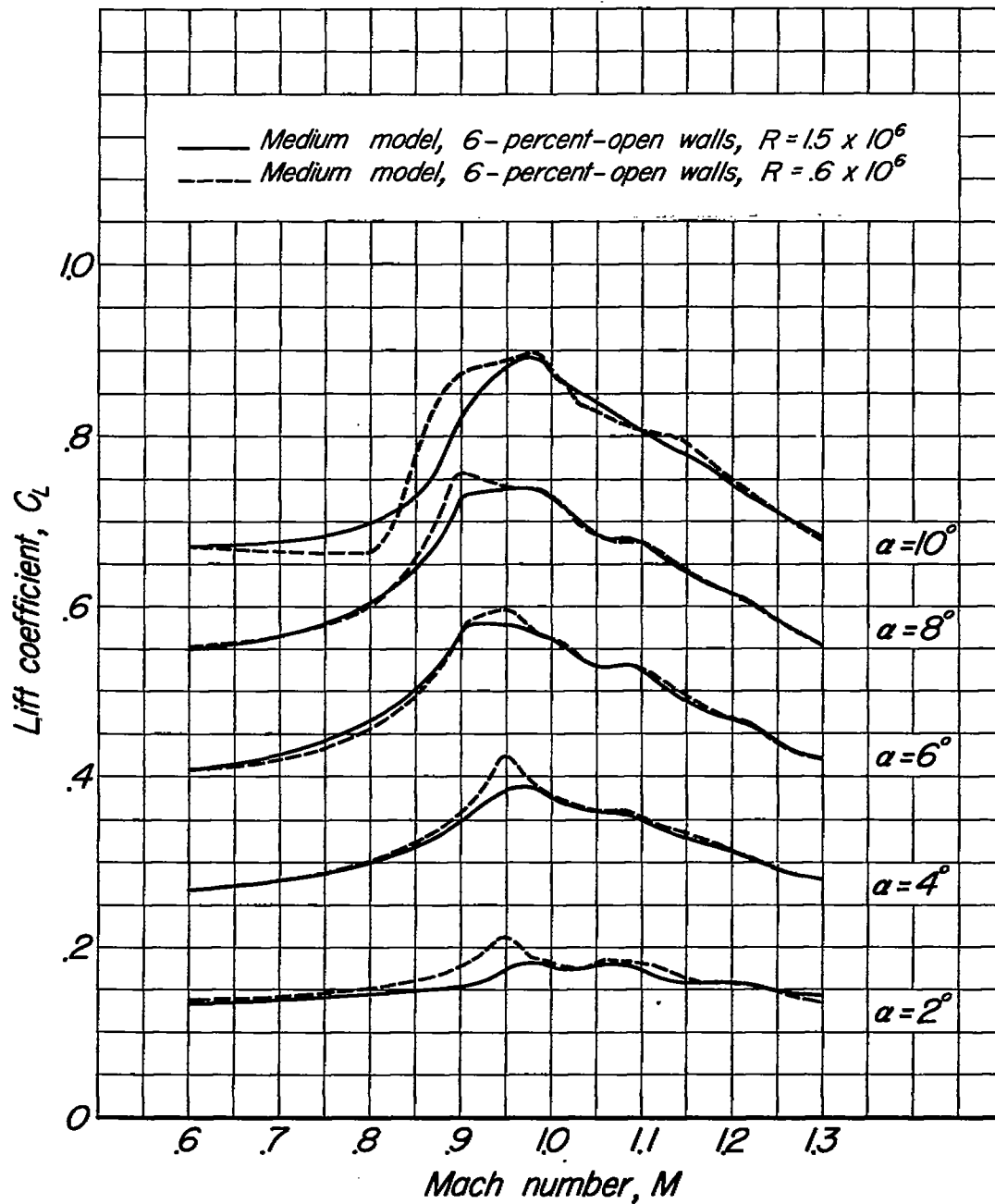
(a) C_L vs. M for constant α

Figure 18.- Effect of Reynolds number on the aerodynamic characteristics as a function of Mach number; medium model.

Legend:
——— Medium model, 6-percent-open walls, R = 1.5 x 10^6
– – – Medium model, 6-percent-open walls, R = .6 x 10^6

$a = 10°$
$a = 8°$
$a = 6°$
$a = 4°$
$a = 2°$
$a = 0$

Drag coefficient, C_D
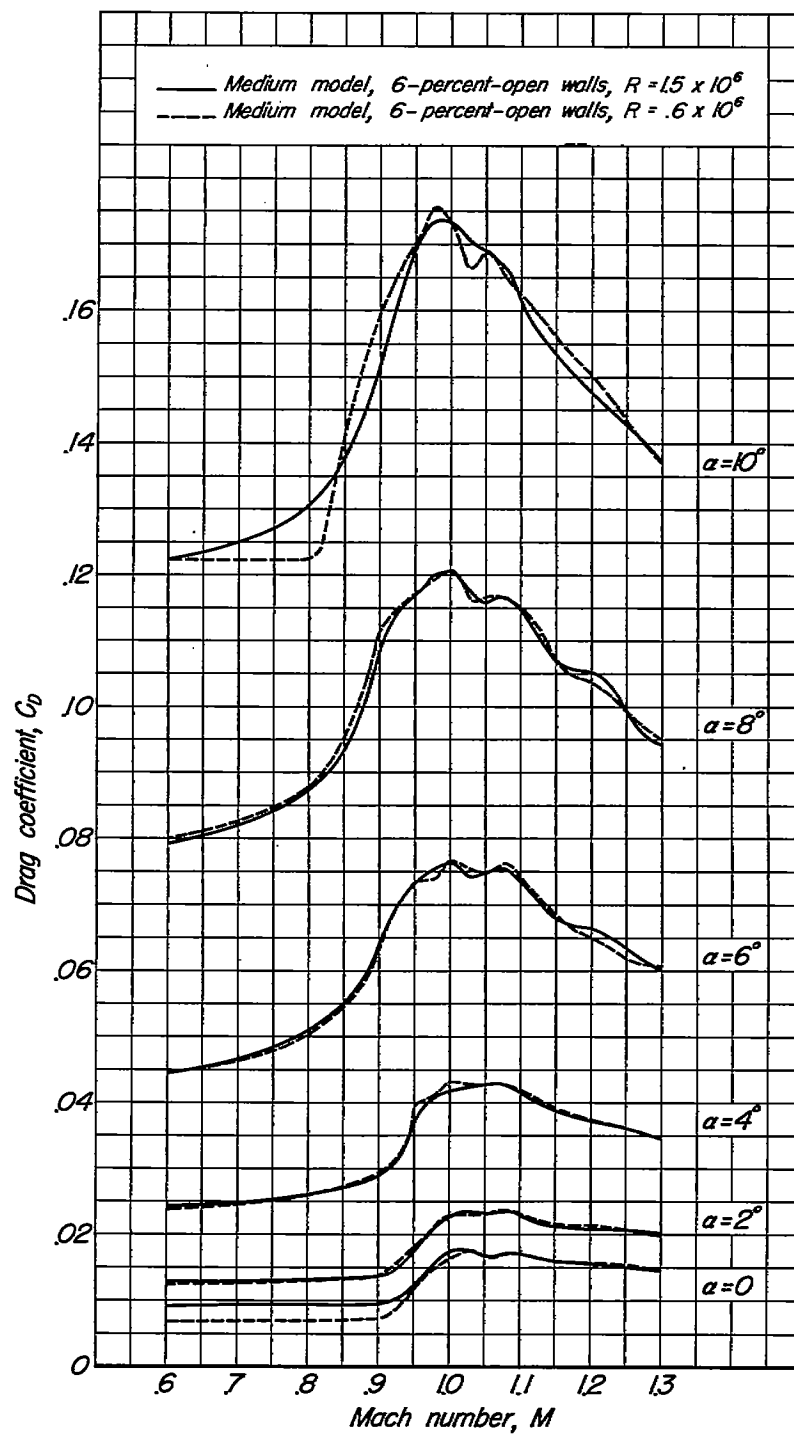
Mach number, M

(b) C_D vs. M for constant a

Figure 18.- Continued.

(c) C_m vs. M for constant α

Figure 18.- Concluded.

(a) C_L vs. M for constant α
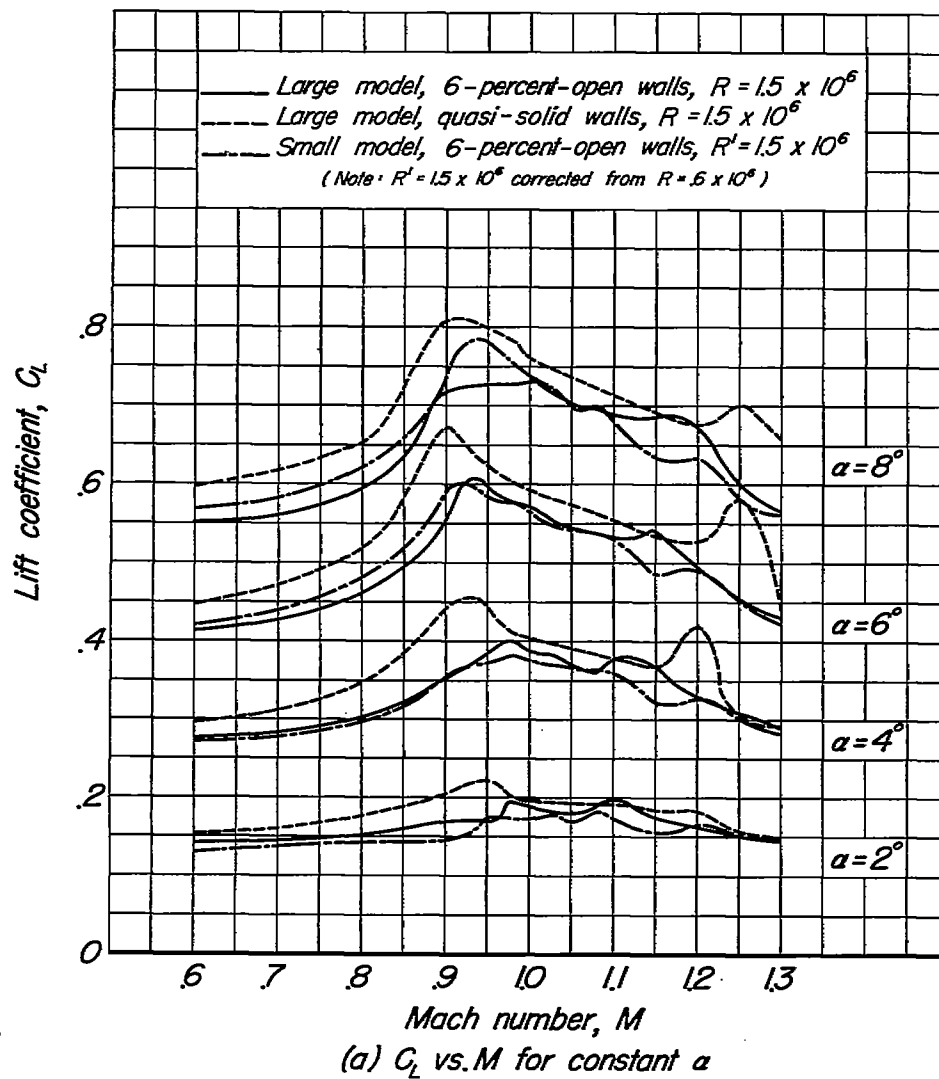
Figure 19.- Effect of test-section-wall solidity on aerodynamic characteristics as a function of Mach number; large model.
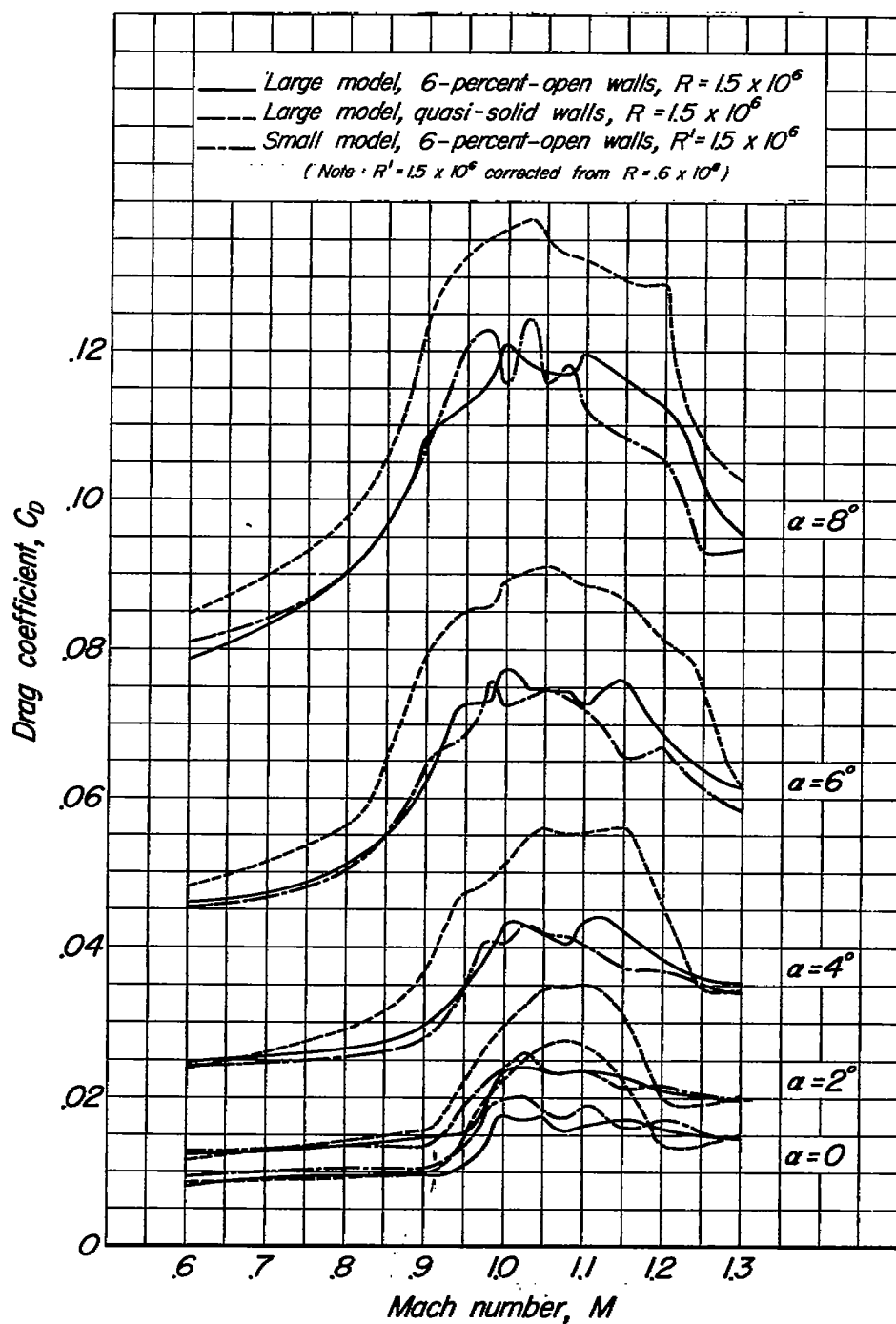
(b) C_D vs. M for constant α

Figure 19.- Continued.
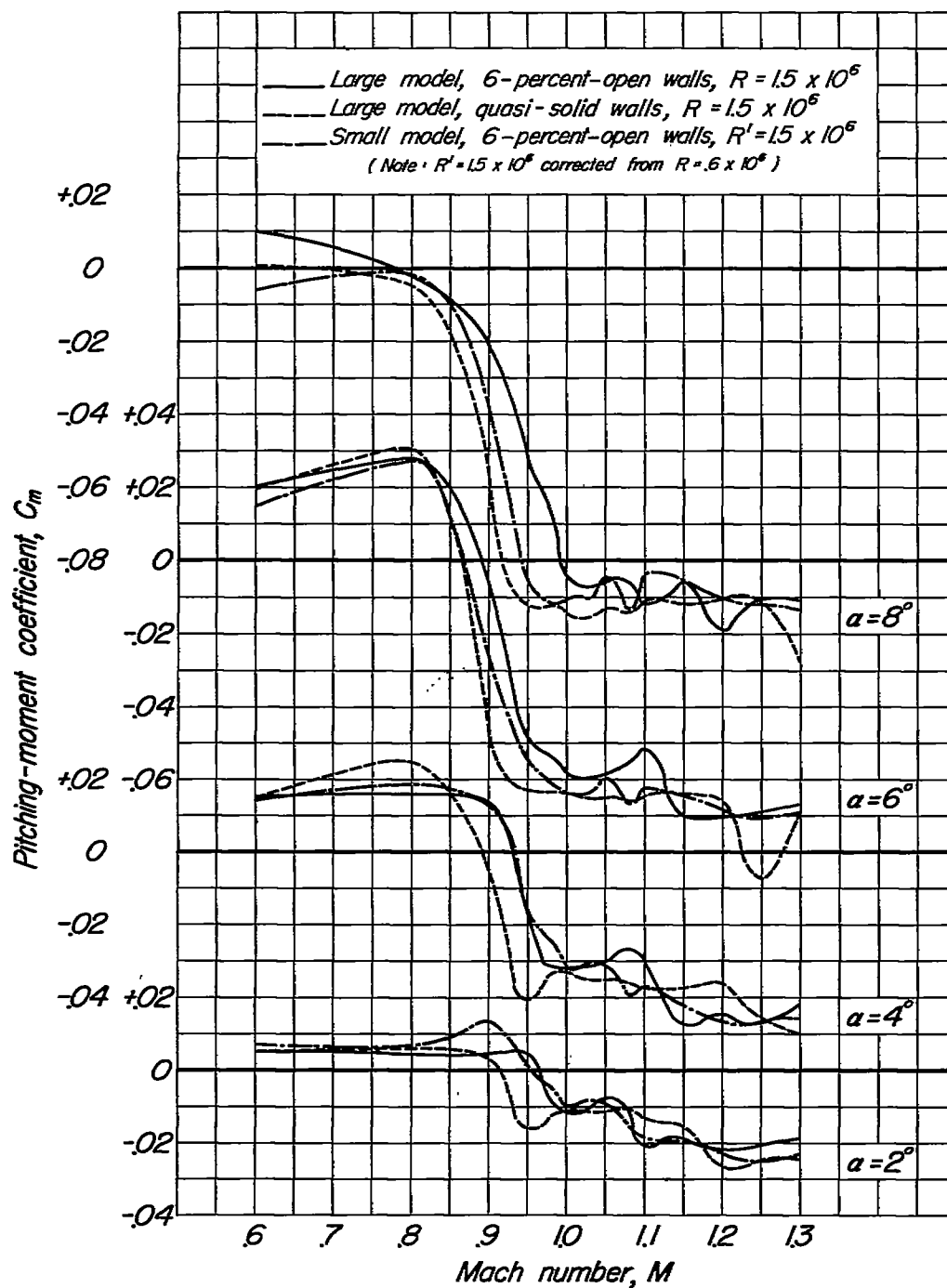
(c) C_m vs. M for constant a

Figure 19.- Concluded.
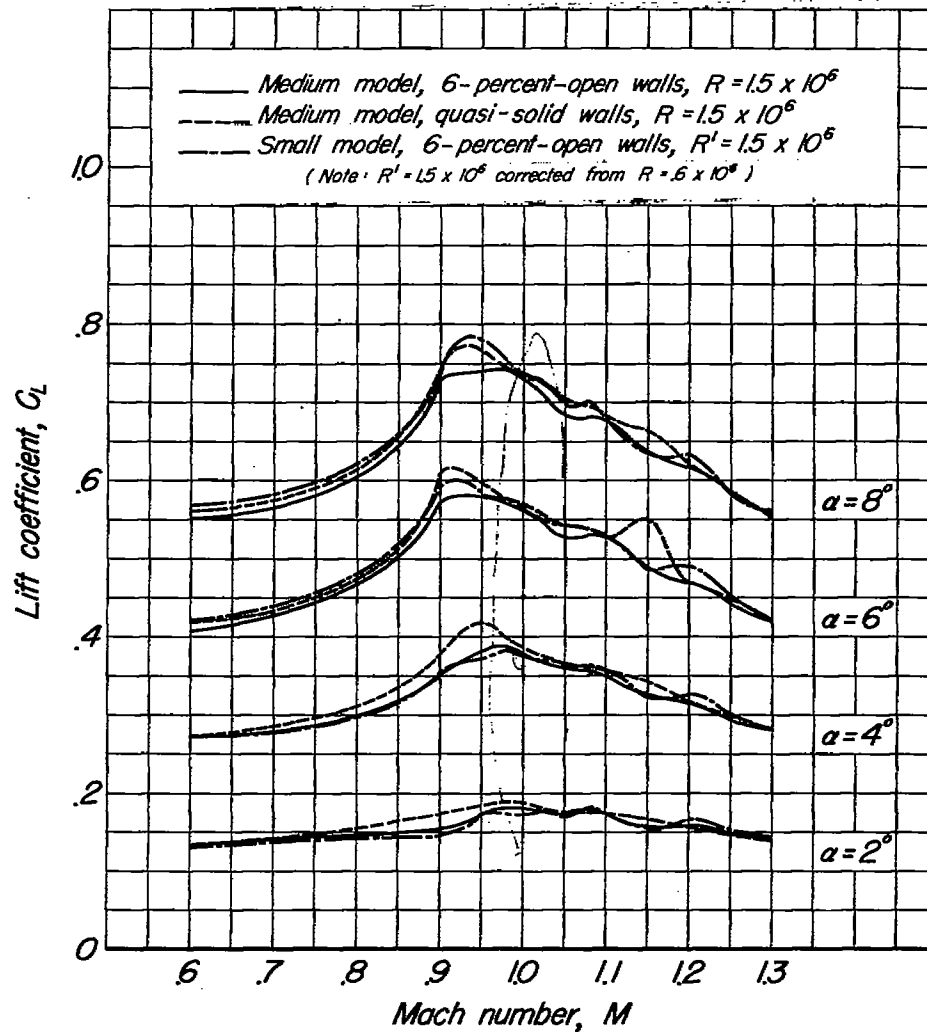
(a) C_L vs. M for constant a

Figure 20.-Effect of test-section-wall solidity on aerodynamic characteristics as a function of Mach number; medium model.
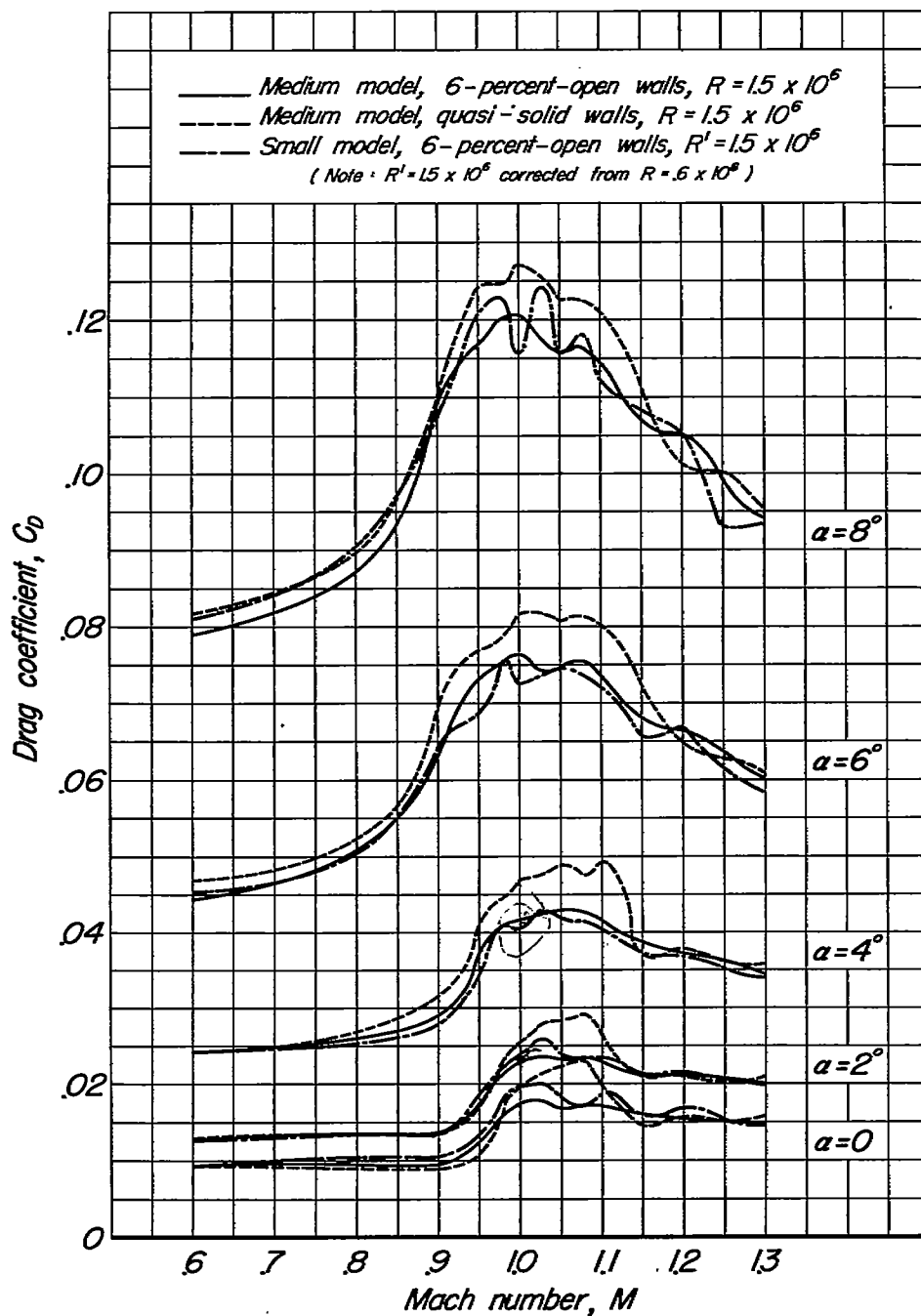
(b) C_D vs. M for constant α

Figure 20.-Continued.
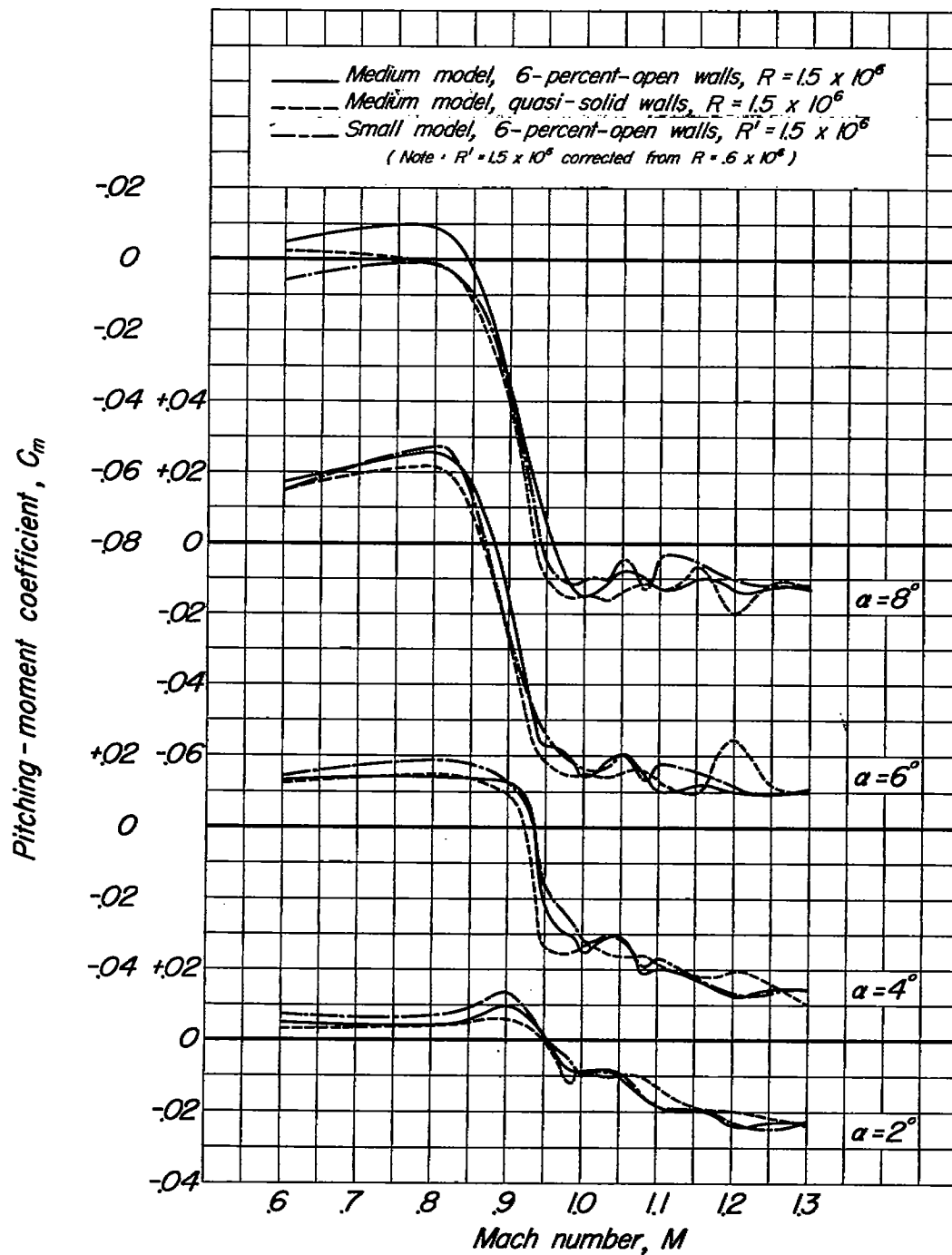
(c) C_m vs. M for constant α

Figure 20.-Concluded.
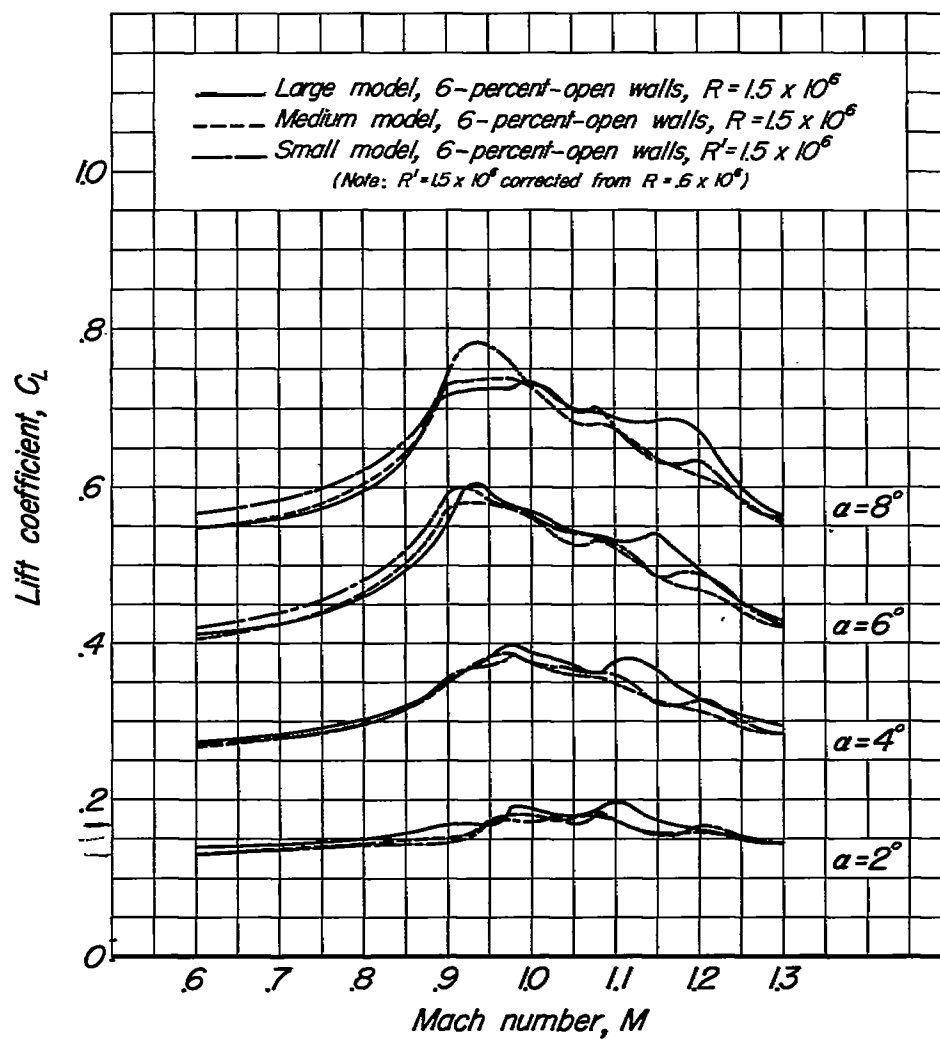
(a) C_L vs. M for constant α

Figure 21.- Variation of aerodynamic characteristics with model size
as a function of Mach number.

Large model, 6-percent-open walls, $R = 1.5 \times 10^6$
Medium model, 6-percent-open walls, $R = 1.5 \times 10^6$
Small model, 6-percent-open walls, $R' = 1.5 \times 10^6$
(Note: $R' = 1.5 \times 10^6$ corrected from $R = .6 \times 10^6$)

Drag coefficient, C_D

$\alpha = 8°$

$\alpha = 6°$

$\alpha = 4°$

$\alpha = 2°$

$\alpha = 0$
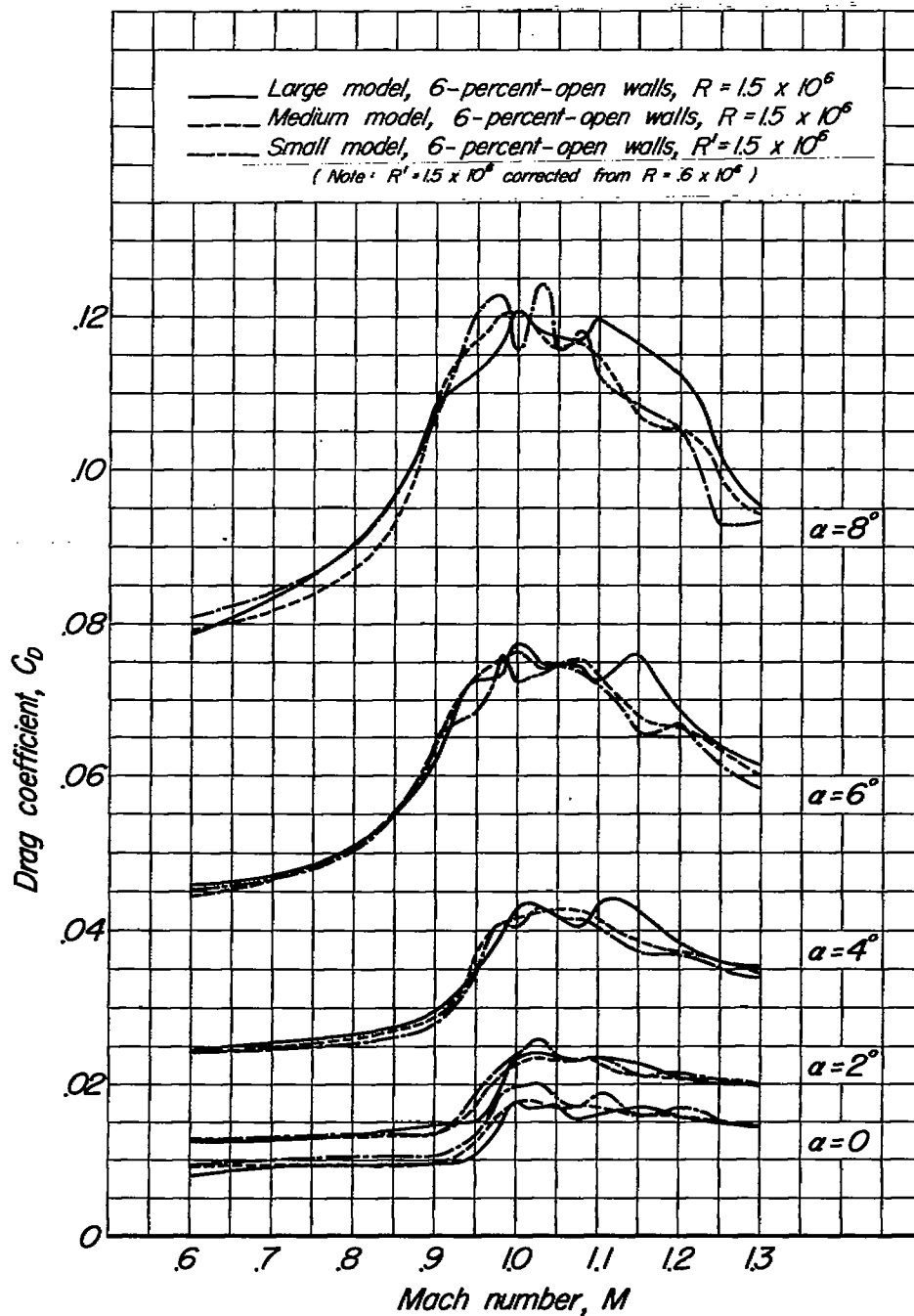
Mach number, M

(b) C_D vs. M for constant α

Figure 21.- Continued.
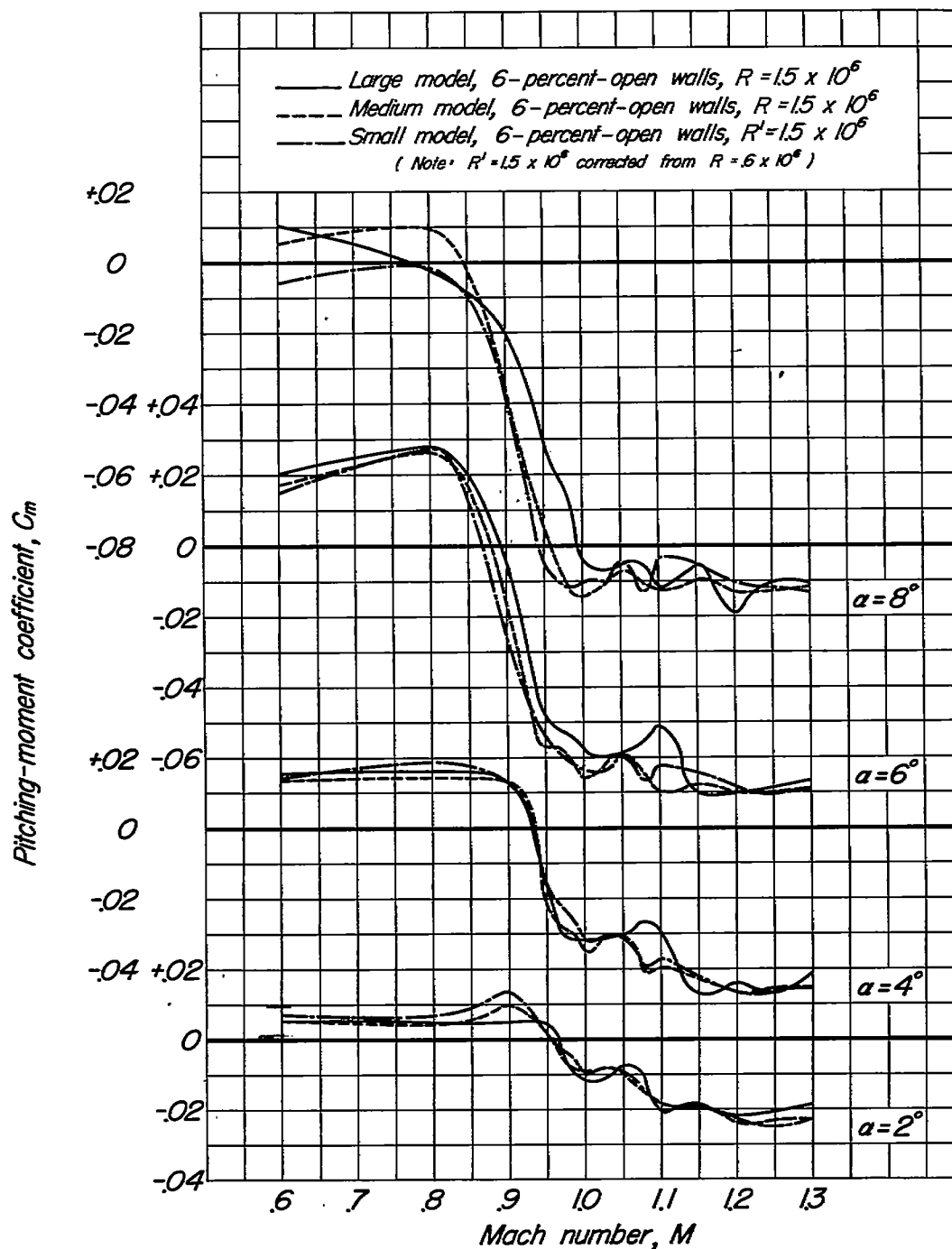
(c) C_m vs. M for constant α

Figure 21.- Concluded.

(a) C_L vs. M for constant α
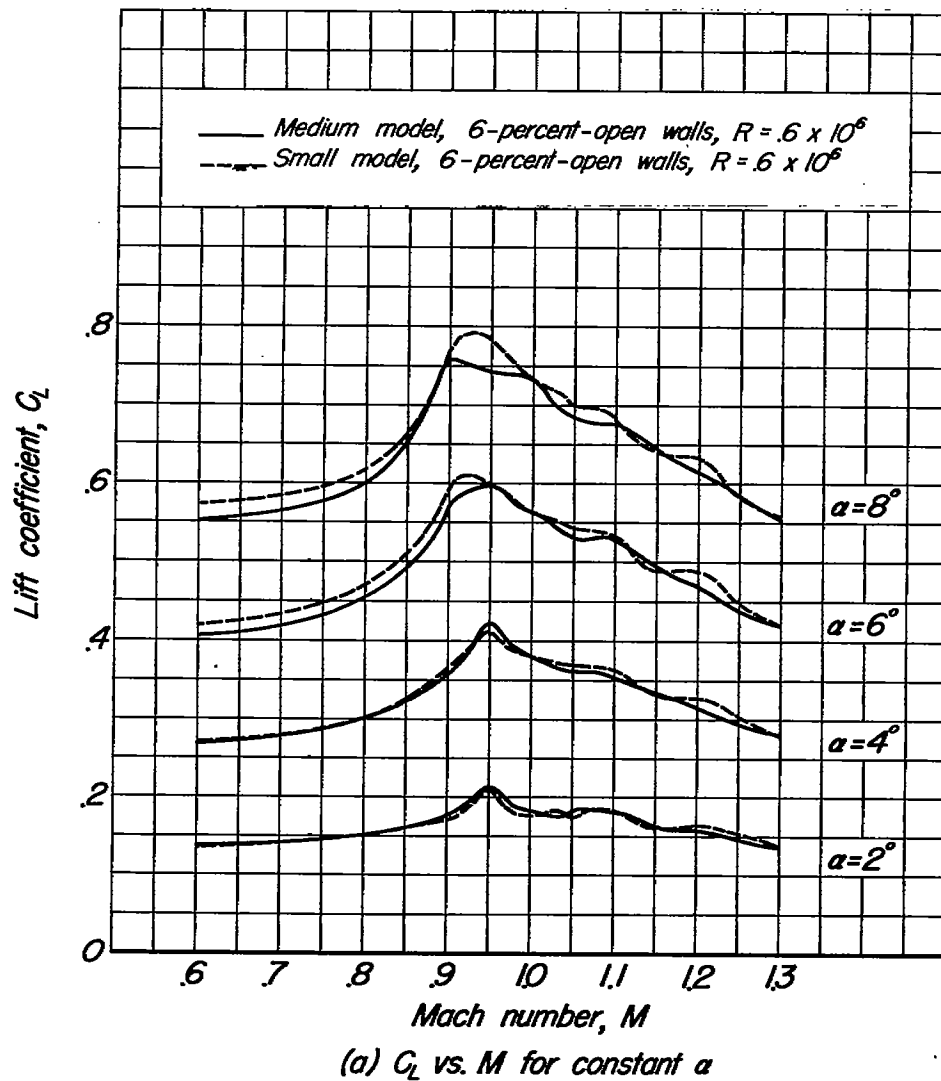
Figure 22.-Variation of aerodynamic characteristics as a function of Mach number showing residual interference on the medium size model.
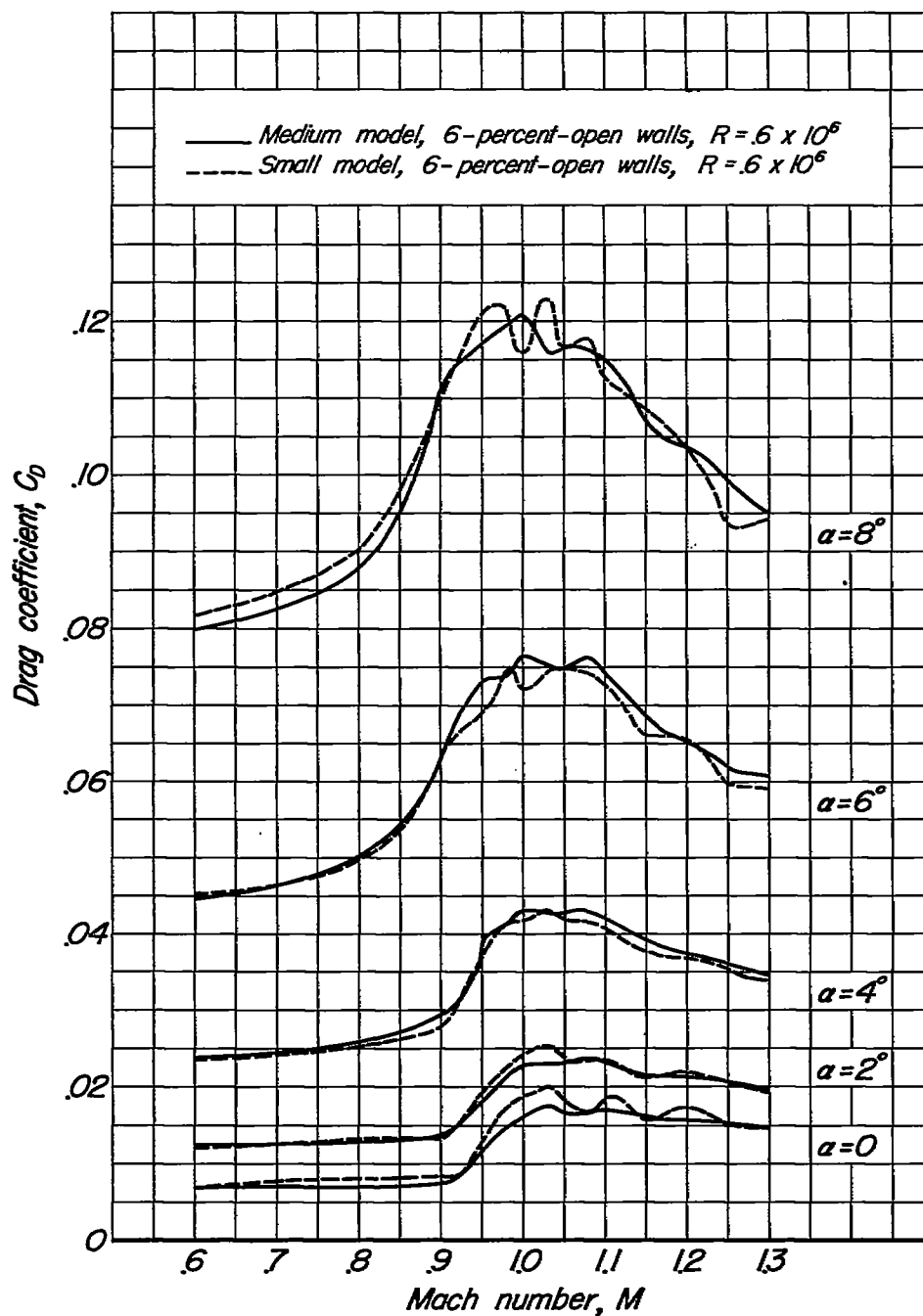
(b) C_D vs. M for constant α

Figure 22.-Continued.
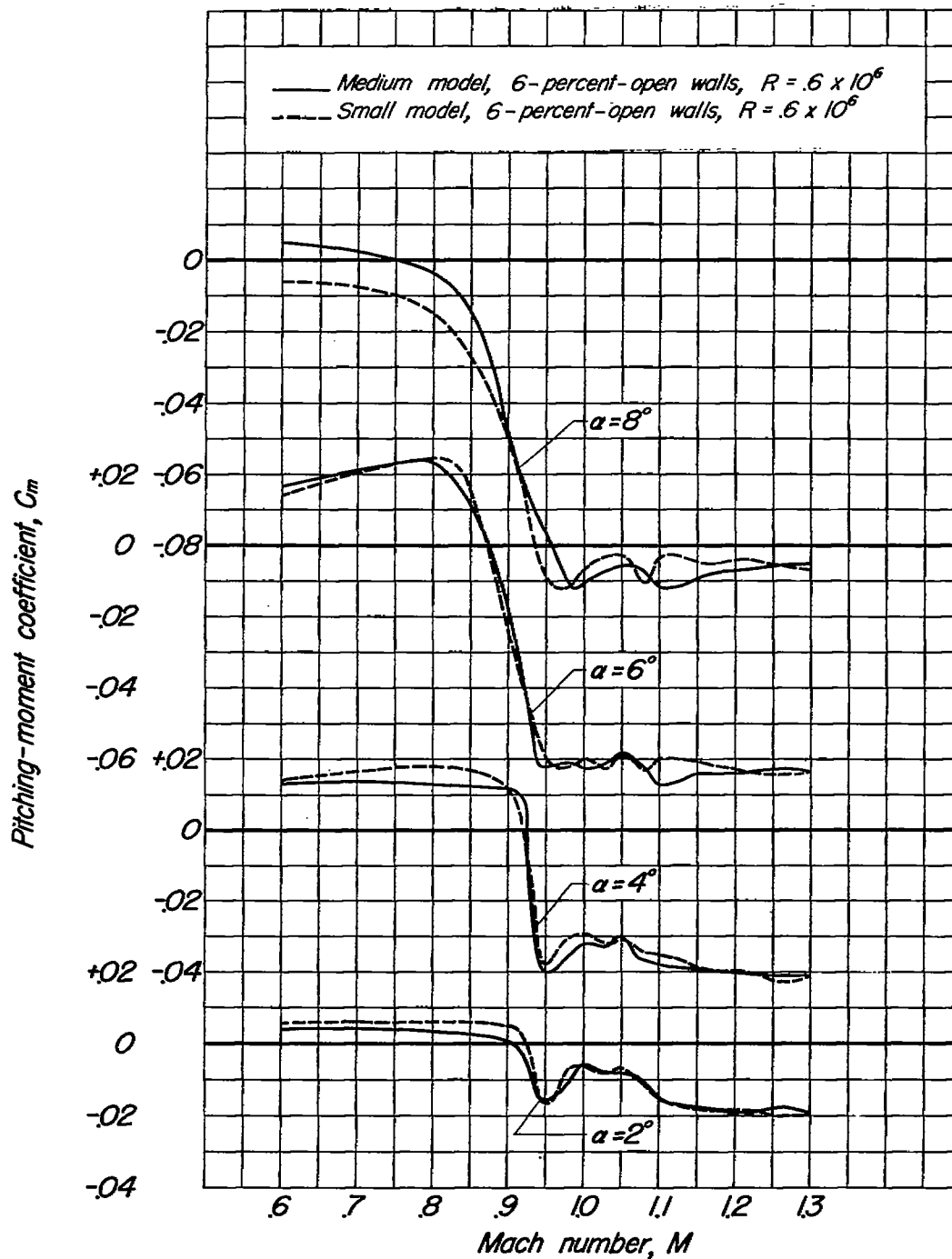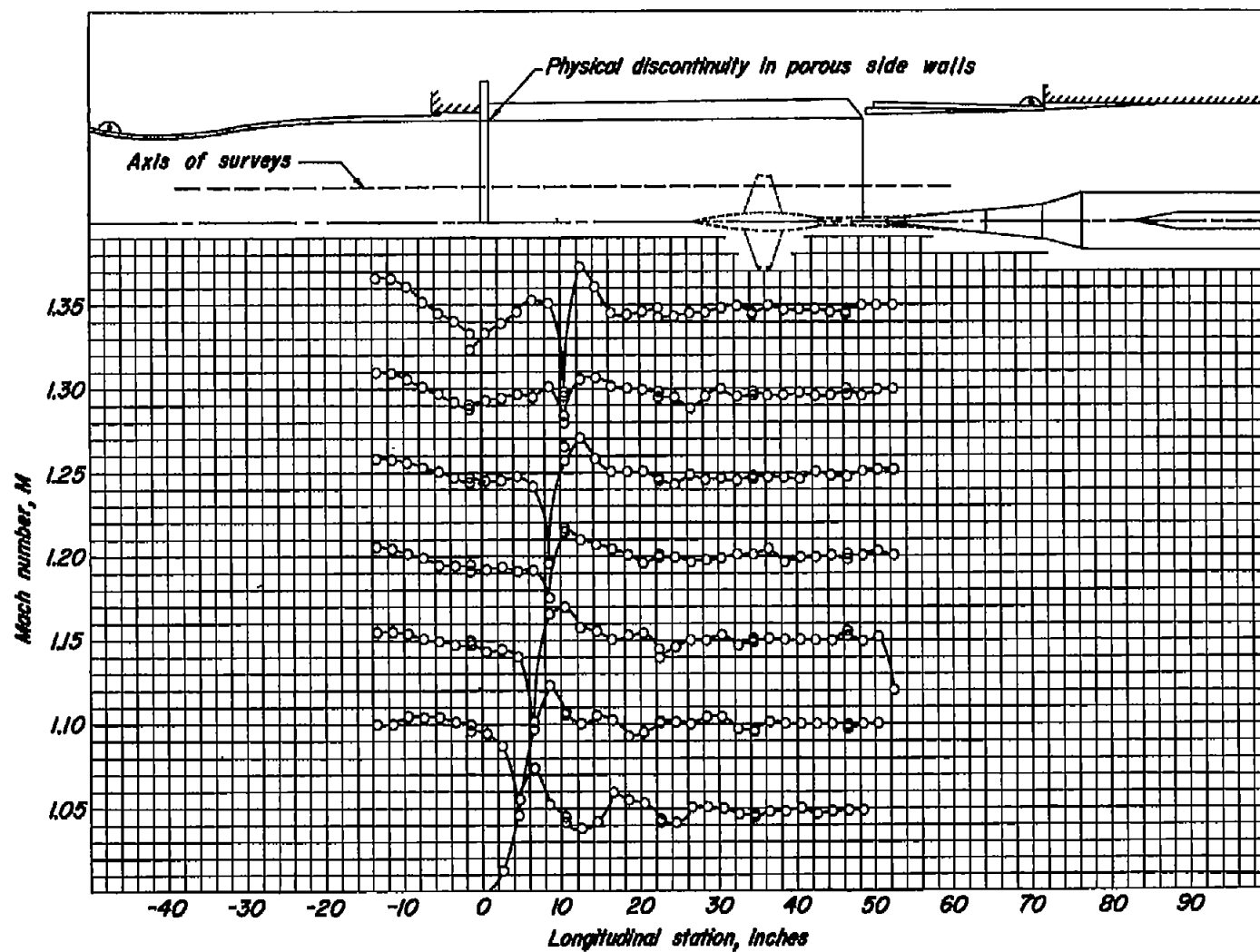
(c) C_m vs. M for constant a

Figure 22.- Concluded.

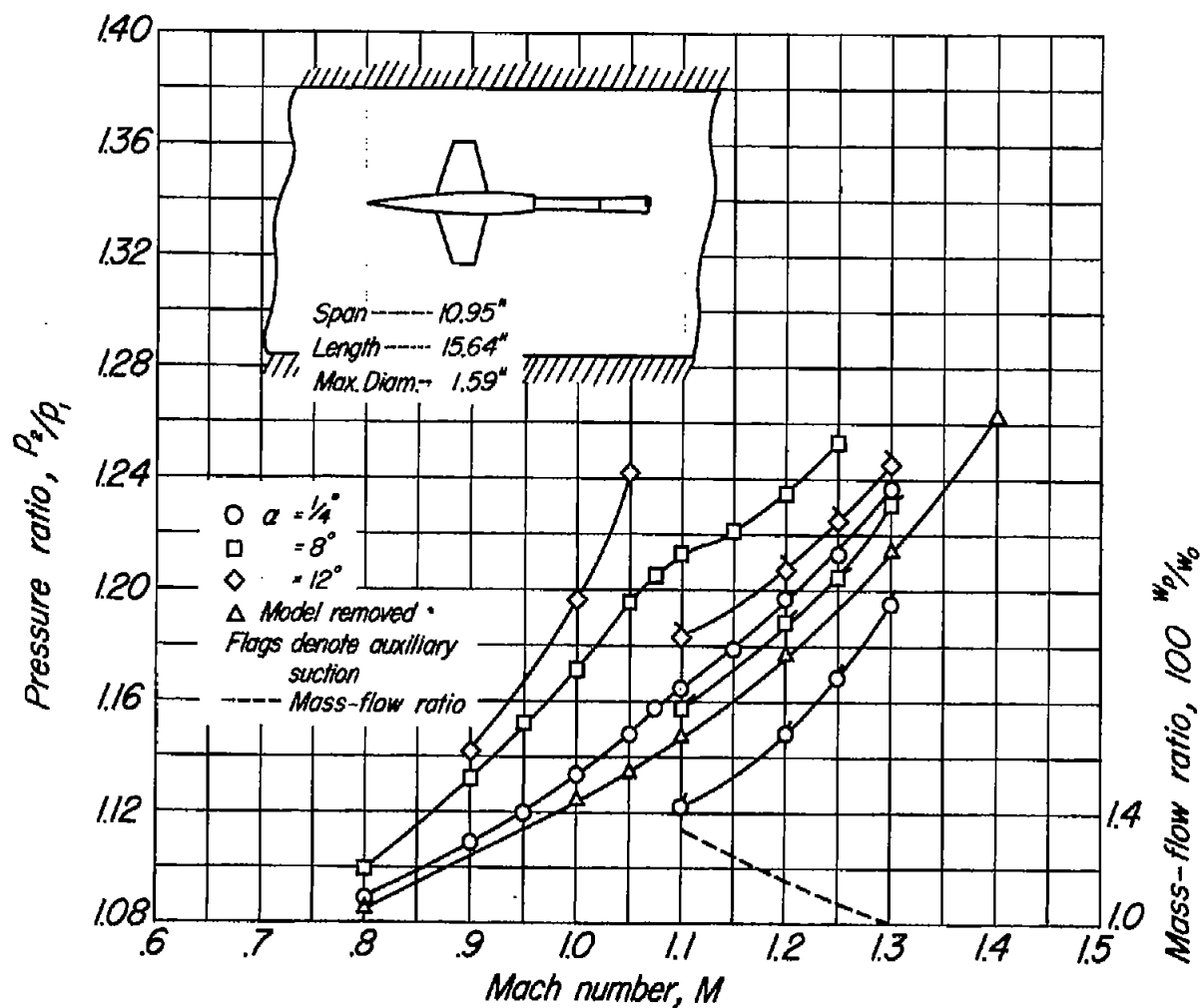Figure 23.- Indication of shock-wave attenuation from pressure surveys.

Figure 24.- Pressure-ratio requirements across main-drive compressor $\left(\frac{p_2}{p_1}, \text{ fig. I.} \right)$
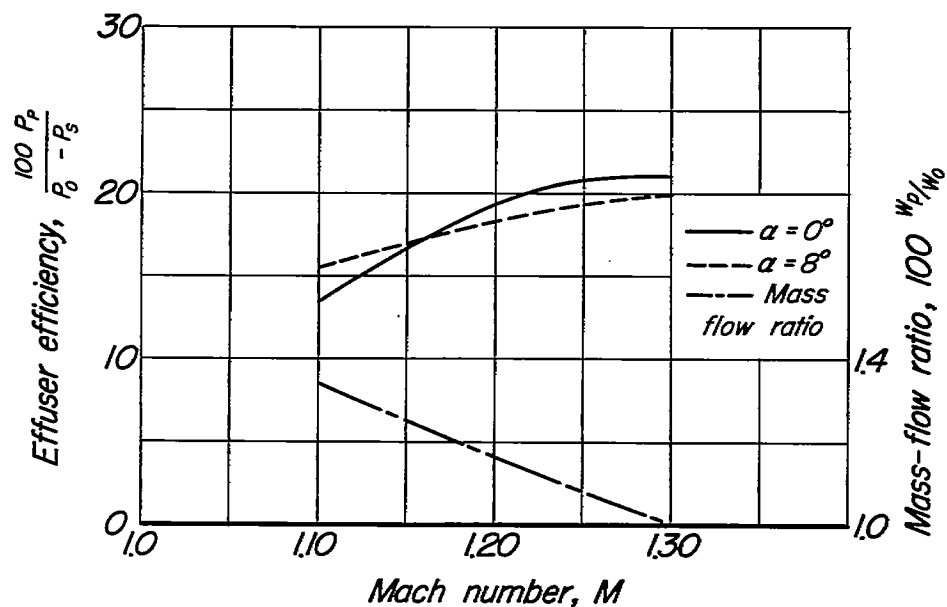
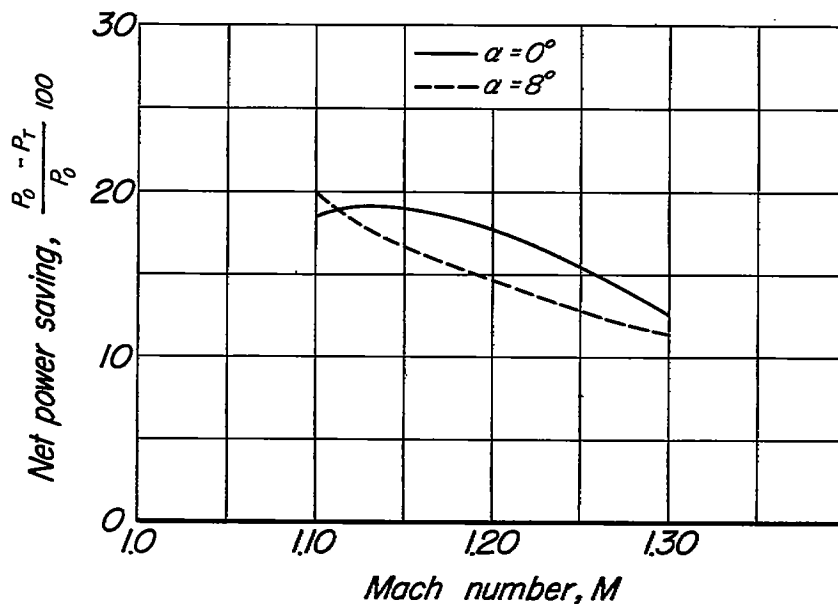Figure 25.- Effuser efficiency based on auxiliary suction power (η = 100 percent).

Figure 26.- Net power saving by use of auxiliary suction (η = 100 percent).